© 2016. Published by The Company of Biologists Ltd | Journal of Cell Science (2016) 129, 4289-4304 doi:10.1242/jcs.194373

RESEARCH ARTICLE

Atg20- and Atg24-family proteins promote organelle autophagy in fission yeast

Dan Zhao[1,2], Xiao-Man Liu[2], Zhong-Qiu Yu[2], Ling-Ling Sun[2], Xingchuang Xiong[3], Meng-Qiu Dong[2] and Li-Lin Du[2,*]

ABSTRACT

Autophagy cargos include not only soluble cytosolic materials but also bulky organelles, such as ER and mitochondria. In budding yeast, two proteins that contain the PX domain and the BAR domain, Atg20 and Atg24 (also known as Snx42 and Snx4, respectively) are required for organelle autophagy and contribute to general autophagy in a way that can be masked by compensatory mechanisms. It remains unclear why these proteins are important for organelle autophagy. Here, we show that in a distantly related fungal organism, the fission yeast *Schizosaccharomyces pombe*, autophagy of ER and mitochondria is induced by nitrogen starvation and is promoted by three Atg20- and Atg24-family proteins – Atg20, Atg24 and SPBC1711.11 (named here as Atg24b). These proteins localize at the pre-autophagosomal structure, or phagophore assembly site (PAS), during starvation. *S. pombe* Atg24 forms a homo-oligomer and acts redundantly with Atg20 and Atg24b, and the latter two proteins can form a hetero-oligomer. The organelle autophagy defect caused by the loss of these proteins is associated with a reduction of autophagosome size and a decrease in Atg8 accumulation at the PAS. These results provide new insights into the autophagic function of Atg20- and Atg24-family proteins.

KEY WORDS: Autophagy, Autophagosome, Atg20, Atg24, PX-BAR, Fission yeast, *Schizosaccharomyces pombe*

INTRODUCTION

Macroautophagy (hereafter autophagy) is an evolutionarily conserved process by which intracellular components are transported into lysosomes or vacuoles using a double-membraned vesicle called an autophagosome. Unicellular eukaryotes, such as yeast, depend heavily on autophagy for their survival when facing starvation. In recent years, diverse roles of autophagy have been uncovered in various aspects of human health, such as cancer, infectious disease and aging (Jiang and Mizushima, 2014).

The molecular machinery driving autophagy has been best characterized in the budding yeast *Saccharomyces cerevisiae* (Xie and Klionsky, 2007; Inoue and Klionsky, 2010; Mizushima et al., 2011; Feng et al., 2014; Ohsumi, 2014). Extensive studies in this organism have identified dozens of autophagy-related (Atg) proteins. Some of the Atg proteins are required for the autophagy of all types of cargo. They are called core Atg proteins and are involved in the biogenesis of autophagosomes. In contrast, other Atg proteins are only required for the autophagy of special cargos but not of general cytosolic proteins. Many of these cargo-specific factors contribute to the autophagy of a single type of cargo, for example by conferring cargo selectivity in a selective autophagy pathway. However, there are also Atg proteins that are required for the autophagy of several different types of special cargos but are dispensable for general autophagy. These include *S. cerevisiae* Atg11, a scaffold protein that binds to many cargo-selectivity factors, and Atg20 and Atg24 (also known as Snx42 and Snx4, respectively), which are two PX-BAR proteins whose exact functions remain mysterious (Inoue and Klionsky, 2010).

S. cerevisiae ATG20 (originally called *CVT20*) and *ATG24* (originally called *CVT13*) genes were first implicated in autophagy when their mutants were isolated in screens for mutants defective in the cytoplasm-to-vacuole targeting (Cvt) pathway, a selective autophagy pathway constitutively transporting the cytosolic hydrolase Ape1 into the vacuole (Nice et al., 2002). In the same study, it was shown that these two genes are also required for the autophagy of peroxisomes (pexophagy). Subsequently, it was shown that they are also required for the efficient autophagy of mitochondria (mitophagy) (Kanki and Klionsky, 2008; Kanki et al., 2009b; Okamoto et al., 2009). Atg20 and Atg24 localize to the pre-autophagosomal structure or phagophore assembly site (PAS) in a manner that is dependent on their binding to phosphatidylinositol 3-phosphate through the PX domain (Nice et al., 2002).

The cellular functions of *S. cerevisiae* Atg20 and Atg24 are not limited to selective autophagy. Combining *atg20*Δ or *atg24*Δ with any one of several Golgi–endosomal-trafficking mutants resulted in synergistic defects in starvation-induced bulk autophagy, suggesting that Atg20 and Atg24 contribute to general autophagy in a way that can be masked by compensatory mechanisms (Ohashi and Munro, 2010; Shirahama-Noda et al., 2013). In addition, Atg20, Atg24 and a paralog of Atg20 – called Snx41 – are required for the endosomal sorting of the SNARE protein Snc1 (Hettema et al., 2003). It is unclear whether Snx41 participates in autophagy. The relationship between the autophagic function and the endosomal sorting function of Atg20 and Atg24 has not been thoroughly investigated.

Few studies have examined the autophagic roles of Atg20- and Atg24-related proteins in species other than *S. cerevisiae*. In the methylotrophic yeast *Pichia pastoris*, the ortholog of Atg24 is required for pexophagy, but the roles of the Atg20- and Snx41-related proteins are unknown (Ano et al., 2005). In the rice-blast fungus *Magnaporthe oryzae*, the ortholog of Atg24 is required for mitophagy (He et al., 2013), whereas an Atg20- and Snx41-related protein is required for pexophagy (Deng et al., 2012, 2013). Mammalian homologs of Atg20 and Atg24 exist (van Weering

[1]PTN Graduate Program, School of Life Sciences, Peking University, Beijing 100871, China. [2]National Institute of Biological Sciences, Beijing 102206, China. [3]National Institute of Metrology, Beijing 100013, China.

*Author for correspondence (dulilin@nibs.ac.cn)

L.-L.D., 0000-0002-1028-7397

Received 24 June 2016; Accepted 6 October 2016

Journal of Cell Science (2016) 129, 4289-4304 doi:10.1242/jcs.194373

et al., 2010), but it is unknown whether they are involved in autophagy.

The fission yeast *Schizosaccharomyces pombe* is an important unicellular eukaryotic model organism and is evolutionarily distant from the budding yeast *S. cerevisiae* (Hoffman et al., 2015). We have previously comprehensively identified and characterized the fission yeast genes that are required for starvation-induced autophagy, and unveiled interesting differences in autophagic mechanisms between the two model yeasts (Sun et al., 2013). For example, unlike its budding yeast counterpart, fission yeast Atg11 is required for general autophagy. Thus, Atg11 dependence cannot be used as a criterion to judge whether a cargo is selectively targeted by autophagy in fission yeast. No systematic analysis on the autophagy of special cargos, such as organelles, has been performed in fission yeast.

In this study, we firstly demonstrated that two types of organelles, ER and mitochondria, are subject to autophagy during nitrogen starvation in fission yeast. To understand whether organelle autophagy has requirements that different from those of general autophagy, we studied the four fission yeast homologs of *S. cerevisiae* Atg20 and Atg24, none of which has been experimentally characterized before. Out of the four proteins, we found that at least three of them, Atg20, Atg24 and Atg24b, play redundant roles in organelle autophagy. We examined their subcellular localization patterns and the protein–protein interactions they engage in, and performed in-depth analysis of the phenotypes of their mutants. Our study sheds new light on the autophagic function of the Atg20- and Atg24-related proteins.

RESULTS

Organelle autophagy is induced by nitrogen starvation in *S. pombe*

To our knowledge, the only report of organelle autophagy in *S. pombe* is the observation that mitochondrial autophagy is required for the survival of a proteasome mutant in quiescent state (Takeda et al., 2010). To examine whether organelle autophagy occurs in wild-type cells, we applied nitrogen starvation treatment, which is a trigger of general autophagy in *S. pombe* (Kohda et al., 2007; Mukaiyama et al., 2009; Sun et al., 2013), and monitored the subcellular localization of two organelle markers, an ER integral membrane protein Ost4 and a mitochondrial matrix protein Sdh2. We used Cpy1 as a vacuole lumen marker (Tabuchi et al., 1997). Under nutrient-rich conditions (+N), neither Ost4 nor Sdh2 showed obvious overlap with Cpy1 (Fig. 1A,B; Fig. S1A). After shifting cells to a nitrogen-free medium (−N) for 12 h, cells became shortened owing to cell division without cell growth (Yanagida et al., 2011; Young and Fantes, 1987), and pronounced colocalization was observed between Ost4–CFP and Cpy1–mCherry and between Sdh2–mCherry and Cpy1–Venus (Fig. 1A,B; Fig. S1A). Starvation-induced vacuole localization of Ost4–CFP and Sdh2–mCherry did not occur in *atg5Δ* cells (Fig. 1A,B; Fig. S1A), indicating that autophagy is required for the relocalization of ER and mitochondrial proteins into the vacuole lumen.

To determine whether other ER and mitochondrial proteins also undergo starvation-induced relocalization to the vacuole, we analyzed the localization patterns of ER-GFP and mito-mCherry, which are fluorescent proteins targeted to ER lumen and mitochondrial matrix by a signal peptide and an ER retrieval sequence (Zhang et al., 2010, 2012), and a mitochondrial targeting sequence (Yaffe et al., 2003), respectively. Under nutrient-rich conditions, neither marker showed overlap with Cpy1, whereas clear colocalization between ER-GFP and Cpy1–mCherry and between mito-mCherry and Cpy1–Venus was observed after nitrogen starvation (Fig. 1C,D; Fig. S1A). In *atg5Δ* cells, both ER-GFP and mito-mCherry failed to enter vacuoles upon starvation (Fig. 1C,D; Fig. S1A). Thus, Atg5-dependent starvation-induced vacuole localization of multiple ER and mitochondrial markers occurs, and most likely reflects the autophagy of these two organelles.

Fluorescent-protein-fused proteins, after entering the vacuole, are attacked by vacuolar proteases and the free forms of fluorescent proteins accumulate owing to resistance to proteases. Thus, to corroborate the imaging data with a biochemical assay, we examined the vacuolar processing of Ost4–CFP and Sdh2–mCherry using immunoblotting analysis. Under nutrient-rich conditions, when probed with antibodies against the fluorescent proteins, Ost4–CFP and Sdh2–mCherry appeared as single bands, whose sizes corresponded to those of the full-length fusion proteins (Fig. 1E,F). For the Ost4–CFP-expressing cells, after 6 h starvation, lower-molecular-mass species that reacted with antibodies against CFP were detected, and one of the new bands ran at a position that was expected for the free CFP (Fig. 1E). Similarly, the processing of Sdh2–mCherry also occurred after starvation (Fig. 1F). As expected, in *atg5Δ* cells, no free CFP or mCherry bands were generated after starvation (Fig. 1E,F).

Taken together, our results indicate that two types of organelles, ER and mitochondria, are delivered into the vacuole through autophagy upon starvation in *S. pombe*. We chose to use the terms of ER autophagy and mitochondrial autophagy, not ER-phagy or mitophagy, to describe these processes, because the latter terms usually refer to selective autophagy pathways (Jin et al., 2013; Okamoto, 2014; Rogov et al., 2014; Sica et al., 2015; Khaminets et al., 2016), and it is not yet clear whether the starvation-induced organelle autophagy processes we observed here were selective or nonselective.

In budding yeast, Atg1 kinase is required for both selective and nonselective autophagy, whereas two Atg1-associated proteins, Atg11 and Atg17, are required for only selective autophagy or only nonselective autophagy, respectively (Inoue and Klionsky, 2010). We found that starvation-induced vacuole localization of Ost4–CFP and Sdh2–mCherry was abolished in fission yeast mutants that lacked either Atg1 or any one of four potential Atg1-associated proteins, including Atg11, Atg13, Atg17 and Atg101 (Fig. S1B,C). Thus, similar to the situation in starvation-induced bulk autophagy (Sun et al., 2013), starvation-induced organelle autophagy requires all five of these Atg proteins in fission yeast.

Atg20, Atg24, Atg24b and Mug186 localize to PAS

Budding yeast Atg20 and Atg24, which are required for organelle autophagy but not general autophagy, are PX-BAR proteins each harboring two membrane-binding domains, a PX domain and a BAR domain (Teasdale and Collins, 2012; van Weering et al., 2010). Our homology searches showed that there are seven PX-BAR proteins in *S. pombe* (Fig. S2A). Four of these seven proteins, SPCC16A11.08 (named Atg20 in PomBase) (McDowall et al., 2015), SPAC6F6.12 (named Atg24 in PomBase), SPBC1711.11 (unnamed in PomBase, hereafter referred to as Atg24b) and SPBC14F5.11c (named Mug186 in PomBase), are more closely related to *S. cerevisiae* Atg20, Atg24 and Snx41. In a phylogenetic tree that we constructed using PX-BAR proteins of representative Ascomycota fungal species, Atg20 and Mug186 fall into the same branch with *S. cerevisiae* Atg20 and Snx41, whereas Atg24 and Atg24b cluster together with *S. cerevisiae* Atg24 in another branch

Journal of Cell Science (2016) 129, 4289-4304 doi:10.1242/jcs.194373

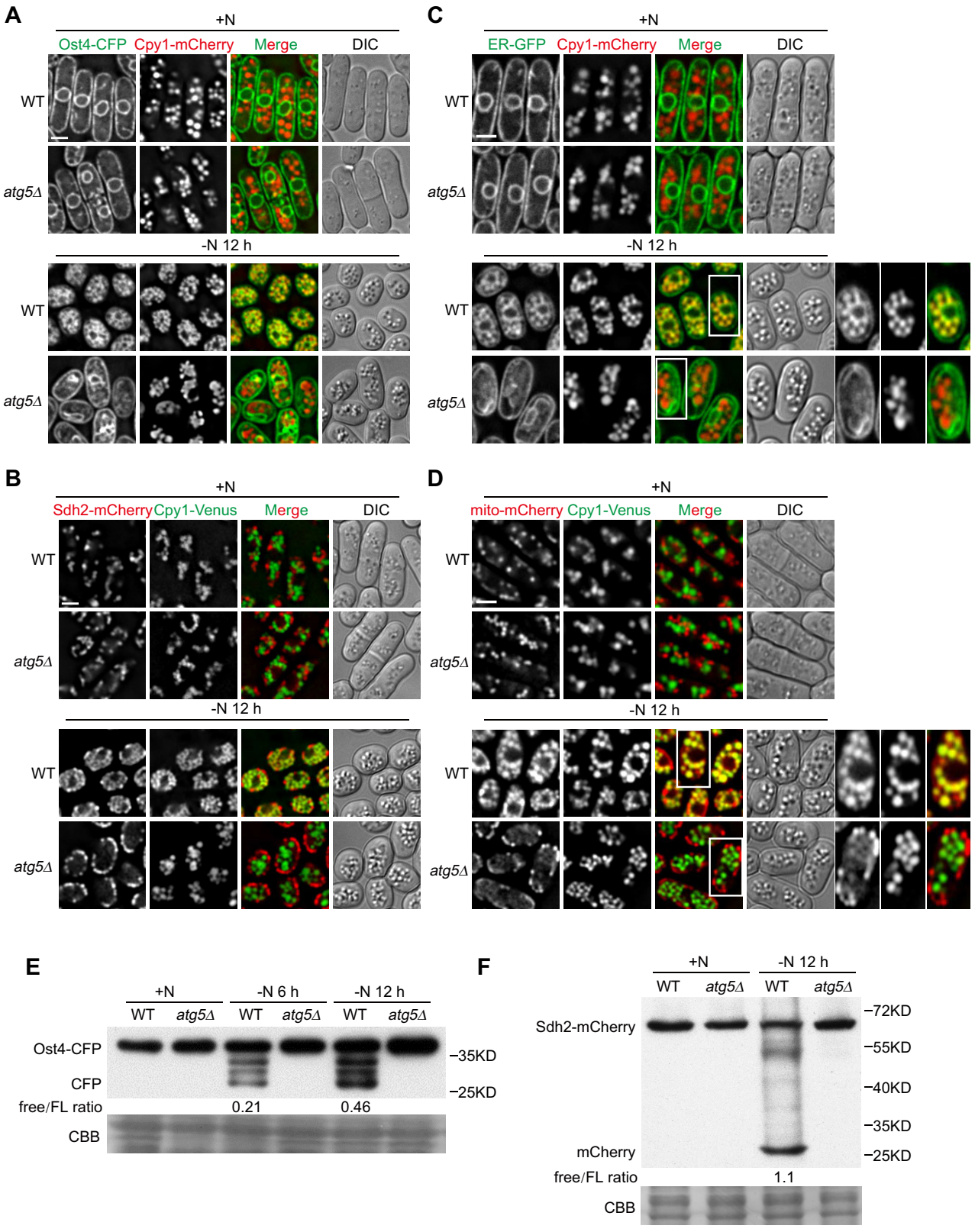

Fig. 1. See next page for legend.

(Fig. S2B). These two branches are more closely related to each other than to the other three branches formed by Vps5, Vps17 and Mvp1 proteins. We will refer to these two branches as the Atg20 family and Atg24 family, respectively. There is at least one Atg20-family protein and one Atg24-family protein in each of the fungal species surveyed. Within the Atg20 family, the two *S. pombe* proteins Atg20 and Mug186 and the two *S. cerevisiae* proteins Atg20 and Snx41 probably have arisen through independent gene

Journal of Cell Science (2016) 129, 4289-4304 doi:10.1242/jcs.194373

Fig. 1. Nitrogen starvation induces the autophagy of ER and mitochondria in fission yeast. (A) An ER marker Ost4–CFP localizes to vacuole lumen upon starvation in an Atg5-dependent manner. Wild-type (WT) and *atg5Δ* cells expressing CFP-tagged Ost4 from the *Pnmt1* promoter were collected before (+N) and after shifting to nitrogen-free medium (–N) for 12 h, and examined by using fluorescence microscopy. Cpy1–mCherry serves as a vacuole lumen marker. DIC, differential interference contrast. (B) A mitochondrial marker, Sdh2–mCherry, localizes to vacuole lumen upon starvation in an Atg5-dependent manner. WT and *atg5Δ* cells expressing endogenously mCherry-tagged Sdh2 were collected before (+N) and after shifting to nitrogen-free medium (–N) for 12 h, and examined by using fluorescence microscopy. Cpy1–Venus serves as a vacuole lumen marker. (C) An ER marker, ER-GFP, localizes to vacuole lumen upon starvation in an Atg5-dependent manner. Wild-type (WT) and *atg5Δ* cells expressing GFP fused with the signal peptide and ER-retention signal of Bip1 from the *bip1* promoter were examined before and after 12 h of starvation. Insets indicate cells shown at higher magnification on the right. (D) A mitochondrial marker, mito-mCherry, localizes to vacuole lumens upon starvation in an Atg5-dependent manner. WT and *atg5Δ* cells expressing mCherry fused with the first 33 amino acids of *S. cerevisiae* Cox4 from the *tub1* promoter were examined before and after 12 h of starvation. White rectangles indicate cells shown at higher magnification on the right. (E,F) Starvation induces the processing of Ost4–CFP (E) and Sdh2–mCherry (F) in an Atg5-dependent manner. Total lysates of WT and *atg5Δ* cells were analyzed by immunoblotting using antibodies that can recognize CFP (E) and mCherry (F). For the lanes where the free form of fluorescent protein appeared, the ratio of the free form of the fluorescent protein versus the full-length tagged protein (free/FL ratio) was determined using the Fiji software. Coomassie Brilliant Blue R-350 (CBB) staining of PVDF membrane after immunodetection was used to control for protein loading and blotting efficiency (Welinder and Ekblad, 2011). Scale bars: 3 µm.

duplication events occurring after the divergence of the ancestors of *S. pombe* and *S. cerevisiae*. Within the Atg24 family, *S. pombe* Atg24 is a closer homolog of *S. cerevisiae* Atg24 than is *S. pombe* Atg24b.

Autophagy proteins in both budding yeast and fission yeast usually localize to a subcellular site called the pre-autophagosomal structure or phagophore assembly site (PAS) when autophagy occurs (Sun et al., 2013; Suzuki and Ohsumi, 2010; Xie and Klionsky, 2007). Budding yeast Atg20 and Atg24 are PAS-localizing proteins (Nice et al., 2002). To assess which fission yeast Atg20- and Atg24-family proteins are involved in autophagy, we tagged their endogenous genes with a C-terminal YFP tag, and examined whether they colocalize with a PAS marker, CFP–Atg8. CFP–Atg8 is diffusely distributed in the cytoplasm under nutrient-rich conditions and, upon starvation, forms bright puncta, where many Atg proteins also accumulate (Sun et al., 2013). Under nutrient-rich conditions, Atg20 formed a few cytoplasmic puncta per cell (Fig. 2A), Atg24 and Mug186 formed dozens of cytoplasmic puncta per cell (Fig. 2B,C), and Atg24b was diffusely distributed in the cytoplasm and the nucleus (Fig. 2D). Starvation induced Atg24b to form a few cytoplasmic puncta per cell (Fig. 2D). After 2 h of starvation, extensive colocalization was observed between CFP–Atg8 puncta and Atg20 puncta, and between CFP–Atg8 puncta and Atg24b puncta (Fig. 2A,D,I), indicating that Atg20 and Atg24b accumulate on the PAS. The large numbers of Atg24 and Mug186 puncta per cell precluded us from reliably determining the extent of their colocalization with CFP–Atg8 puncta. In budding yeast, most of the cytoplasmic puncta formed by Atg24, Snx41 and Atg20 are abolished in a *vps38*Δ mutant (Hettema et al., 2003). Vps38 is a complex-specific subunit of the phosphatidylinositol 3-kinase complex II, which generates phosphatidylinositol 3-phosphate at the endosome (Kihara et al., 2001). We hypothesized that, by using a *vps38Δ* fission yeast mutant background, we could eliminate the endosomal accumulation of Atg20- and Atg24-family proteins and better visualize their localization to the PAS, especially for Atg24 and Mug186. Indeed, in *vps38Δ* cells grown under nutrient-rich conditions, Atg20 no longer formed cytoplasmic puncta (Fig. 2E), and the numbers of puncta formed by Atg24 and Mug186 dramatically decreased (Fig. 2F,G). After starvation, most of the CFP–Atg8 puncta were found to colocalize with the puncta formed by Atg20, Atg24 and Atg24b (Fig. 2E,F,H,I). In contrast, only a minority of CFP–Atg8 puncta overlapped with Mug186 puncta (Fig. 2G,I). PAS localization of Atg20- and Atg24-family proteins should require Atg14, which is the autophagy-specific subunit of the phosphatidylinositol 3-kinase complex I that generates phosphatidylinositol 3-phosphate at the PAS (Kihara et al., 2001). Indeed, puncta formation by these four proteins was completely abolished in *atg14Δ vps38Δ* double-mutant cells (Fig. S3A), in which an Atg14-independent PAS marker, Atg17, still formed starvation-induced puncta (Fig. S3B). Thus, we concluded that all four *S. pombe* Atg20- and Atg24-family proteins localize to the PAS. Atg20, Atg24 and Atg24b have especially pronounced association with the PAS, implying that they play direct roles in autophagy. We next examined whether deleting the genes encoding these four proteins causes autophagy defects.

Atg20, Atg24 and Atg24b act redundantly to promote ER autophagy in *S. pombe*

Because of their sequence similarities, we hypothesized that functional redundancy might exist between Atg20, Atg24, Atg24b and Mug186. Thus, we constructed a quadruple deletion mutant that lacked all four proteins. We first analyzed whether the quadruple mutant has a defect in general autophagy by monitoring the processing of Tdh1–YFP (Fig. 3A). Tdh1 is the major form of fission yeast glyceraldehyde-3-phosphate dehydrogenase (GAPDH) (Morigasaki et al., 2008) and has been used as a representative marker for nonselective bulk autophagy (Sun et al., 2013). Free YFP was generated after starvation in wild type but not in an *atg5Δ* mutant. Wild-type levels of Tdh1–YFP processing occurred in the quadruple mutant, indicating that general autophagy is normal in the absence of Atg20, Atg24, Atg24b and Mug186.

Next, we investigated whether these four proteins participate in organelle autophagy. We first examined the behavior of the ER marker Ost4–CFP by imaging analysis and found that starvation-induced entry of Ost4–CFP into vacuoles was dramatically impeded in the quadruple-mutant cells (Fig. 3B). Similarly, the processing of Ost4–CFP was reduced in the quadruple mutant (Fig. 3C). Thus, the autophagic delivery of ER into the vacuole is defective in the absence of these four proteins.

To further characterize which of these four proteins are involved in this process, we generated single mutants that lacked one of Atg20, Atg24, Atg24b and Mug186, and examined the localization of the other ER marker ER–GFP upon starvation (Fig. 3D). We observed wild-type-like colocalization between ER-GFP and Cpy1 after 12 h of starvation in all four single mutants, suggesting that the ER autophagy defect of the quadruple mutant is due to the loss of more than one protein. We then examined double mutants that lacked two of the four proteins and found that the vacuole localization of ER-GFP was strongly diminished in *atg20Δ atg24Δ* and *atg24Δ atg24bΔ* strains, but not in the other four double mutants (Fig. 3D), suggesting that Atg20, Atg24 and Atg24b play crucial but redundant functions in ER autophagy. Finally, we examined triple mutants that lacked three of the proteins. Vacuole localization of ER-GFP was defective in three of the four triple mutants (Fig. 3D). The exception was *atg20Δ atg24bΔ mug186Δ*, suggesting that Atg24 can fully support ER autophagy in the absence of the other

Journal of Cell Science (2016) 129, 4289-4304 doi:10.1242/jcs.194373

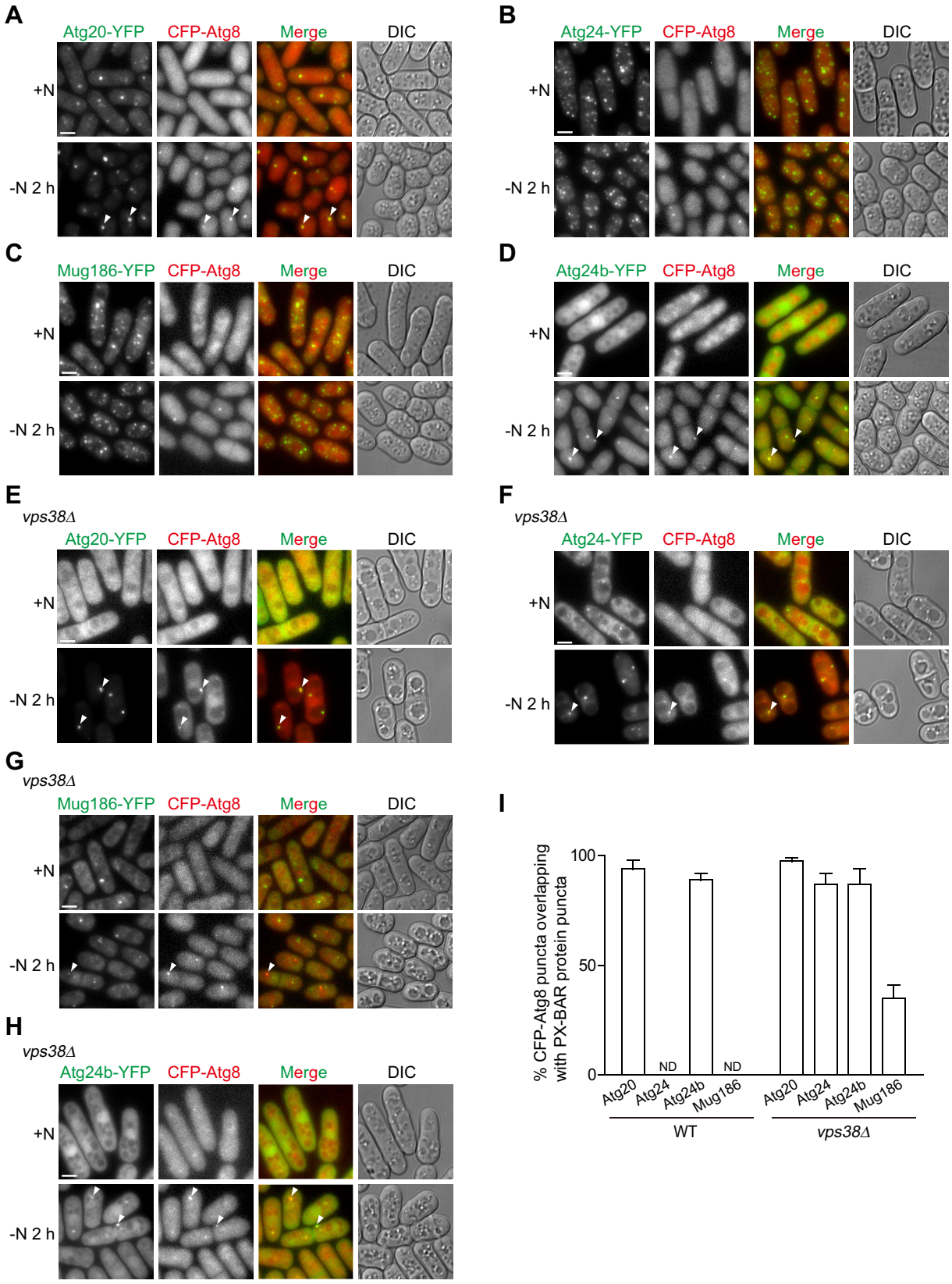

Fig. 2. Atg20, Atg24, Atg24b and Mug186 form puncta at the PAS during starvation. (A–D) Location of Atg20–YFP (A), Atg24–YFP (B), Mug186–YFP (C) and Atg24b–YFP (D) before and 2 h after starvation in the wild-type background. YFP-tagged proteins were expressed from endogenous promoters. CFP–Atg8 serves as a marker for the starvation-induced PAS. Arrowheads point to representative puncta where colocalization with CFP–Atg8 occurs. (E–H) Location of Atg20–YFP (E), Atg24–YFP (F), Mug186–YFP (G) and Atg24b–YFP (H) before and 2 h after starvation in the *vps38Δ* background. (I) Quantification of the percentages of CFP–Atg8 puncta that overlapped with puncta formed by Atg20- and Atg24-family proteins in starved cells (mean±s.e.m.; 100 Atg8 puncta were examined each time). ND, not determined. +N, nitrogen-containing medium; –N, nitrogen-starvation medium. Scale bars: 3 µm.

Journal of Cell Science (2016) 129, 4289-4304 doi:10.1242/jcs.194373

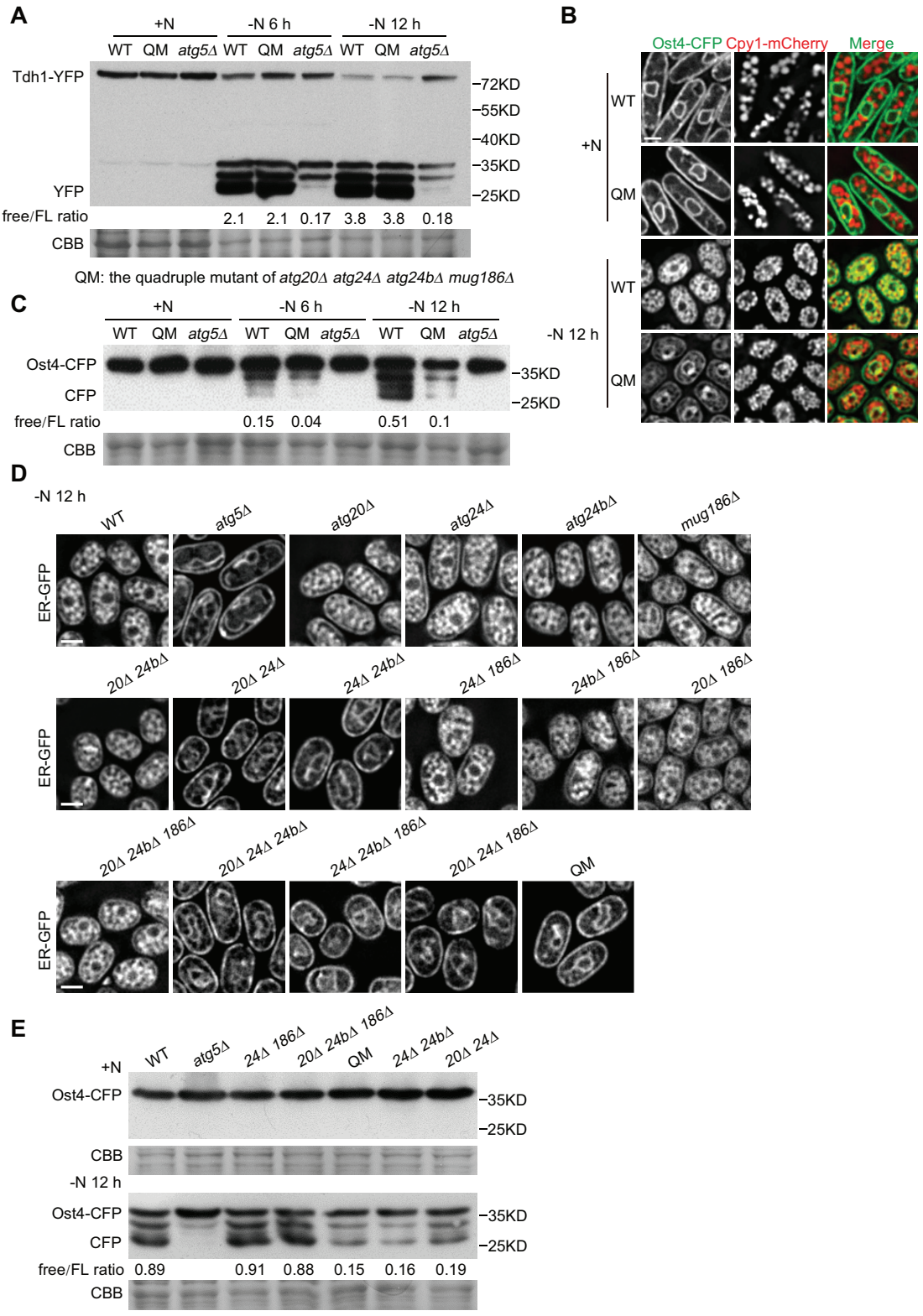

Fig. 3. Atg20, Atg24 and Atg24b are important for ER autophagy but not for general autophagy. (A) Starvation-induced processing of Tdh1–YFP was monitored in the wild type (WT), *atg5Δ* mutant and quadruple mutant (QM) that lacked all four Atg20- and Atg24-family proteins. Cells expressing YFP-tagged Tdh1 from the *Pnmt1* promoter were collected before and after starvation, and the total lysates were analyzed by immunoblotting using an antibody that recognizes YFP. (B) Starvation-induced vacuole localization of Ost4–CFP was diminished in the quadruple mutant. (C) Starvation-induced processing of Ost4–CFP was reduced in the quadruple mutant. Cell lysates were analyzed by immunoblotting with an antibody that recognizes CFP. (D) Starvation-induced vacuole localization of ER-GFP was monitored in all combinations of single, double, triple and quadruple mutants that lacked the indicated combinations of Atg20- and Atg24-family proteins. 20, Atg20; 24, Atg24; 24b, Atg24b; 186, Mug186. (E) Starvation-induced processing of Ost4–CFP was monitored in selected double and triple mutants. The free/FL ratios were calculated as described in Fig. 1. +N, nitrogen-containing medium; –N, nitrogen-starvation medium. Scale bars: 3 µm.

Journal of Cell Science (2016) 129, 4289-4304 doi:10.1242/jcs.194373

three proteins. Among the double and triple mutants that lacked Atg24, only the *atg24Δ mug186Δ* double mutant behaved like wild type. Thus, in the absence of Atg24, both Atg20 and Atg24b, but not Mug186, become important. To further confirm these results, we analyzed the processing of Ost4–CFP (Fig. 3E). Consistent with the imaging results obtained with the ER-GFP marker, the *atg20Δ atg24bΔ mug186Δ* triple mutant and *atg24Δ mug186Δ* double mutant behaved like wild type, indicating that either Atg24 alone or the combination of Atg20 and Atg24b can fully support ER autophagy. Starvation-induced processing of Ost4–CFP was diminished in *atg20Δ atg24Δ* and *atg24Δ atg24bΔ* double mutants. The severity of the defect of these two double mutants was similar to that of the quadruple mutant, suggesting that the remaining proteins in these two double mutants, either the combination of Mug186 and Atg24b or the combination of Mug186 and Atg20, cannot even partially fulfill the autophagic function performed by Atg24 or the combination of Atg20 and Atg24b.

In conclusion, we found that, among the four Atg20- and Atg24-family fission yeast proteins, at least three, Atg20, Atg24 and Atg24b, contribute to ER autophagy in a redundant manner. Either Atg24 alone or Atg20 and Atg24b together are sufficient for ER autophagy.

Atg20, Atg24 and Atg24b act redundantly to promote mitochondrial autophagy in *S. pombe*

We hypothesized that Atg20, Atg24 and Atg24b function in mitochondrial autophagy in a redundant manner, similar to the way they act in ER autophagy. Thus, we examined a number of selected double and triple mutants. Consistent with the findings for ER autophagy, the vacuolar entry of the mitochondrial marker mito-mCherry was impeded in *atg20Δ atg24Δ* and *atg24Δ atg24bΔ* double mutants, but not in the *atg24Δ mug186Δ* double mutant and *atg20Δ atg24bΔ mug186Δ* triple mutant (Fig. 4A). Similarly, the processing of Sdh2–mCherry was defective in *atg20Δ atg24Δ* and *atg24Δ atg24bΔ* double mutants, but not the in *atg24Δ mug186Δ* double mutant and the *atg20Δ atg24bΔ mug186Δ* triple mutant (Fig. 4B). Taken together, these data demonstrate that, like ER autophagy, mitochondrial autophagy is promoted redundantly by Atg24, Atg20 and Atg24b. Atg24 appears to be sufficient by itself; in its absence, the mitochondrial autophagy-promoting function can be fulfilled equally well by the combined actions of Atg20 and Atg24b.

Fission yeast Atg20- and Atg24-family proteins form multiple oligomers

In *S. cerevisiae*, Atg20- and Atg24-family proteins engage in heterotypic interactions, such as those between Atg24 and Atg20 and between Atg24 and Snx41, as well as homotypic interactions, such as that of Atg24 (Hettema et al., 2003; Nice et al., 2002). Our analysis of double and triple mutants indicates that Atg20 alone or Atg24b alone is insufficient for organelle autophagy, but the presence of both is sufficient. One explanation is that these two proteins act together in a hetero-oligomer. Therefore, we examined the physical interactions between the Atg20- and Atg24-family fission yeast proteins. We first performed affinity purification coupled with mass spectrometry (AP-MS) analysis and observed co-purification between Atg20 and Atg24, between Atg20 and Atg24b, and between Atg24 and Mug186 (Fig. 5A). These interactions were confirmed by performing coimmunoprecipitation

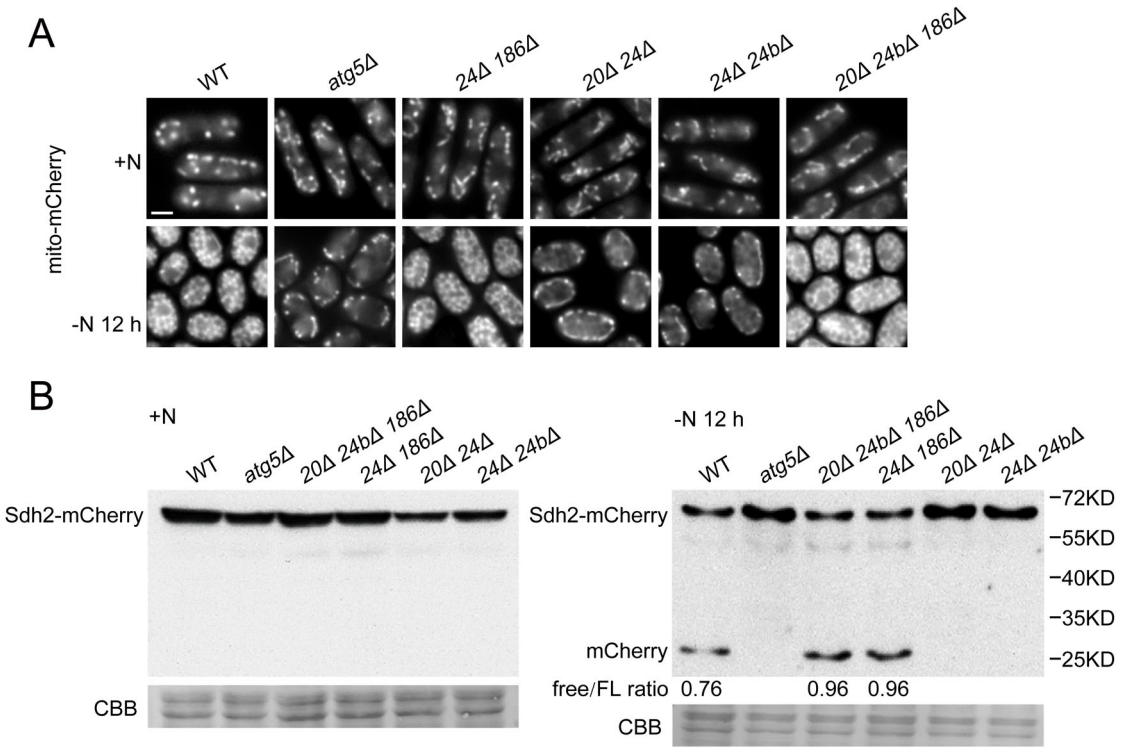

Fig. 4. Mitochondrial autophagy is promoted in a redundant manner by Atg20, Atg24 and Atg24b. (A) Starvation-induced vacuole localization of mito-mCherry was monitored in selected double and triple mutants. 20, Atg20; 24, Atg24; 24b, Atg24b; 186, Mug186. +N, nitrogen-containing medium; –N, nitrogen-starvation medium. Scale bar: 3 µm. (B) Starvation-induced processing of Sdh2–mCherry was monitored in selected double and triple mutants. Coomassie Brilliant Blue R-350 (CBB) staining of PVDF membrane after immunodetection was used to control for protein loading and blotting efficiency. The free/FL ratios were calculated as described in Fig. 1.

Journal of Cell Science (2016) 129, 4289-4304 doi:10.1242/jcs.194373

A

Bait: Atg20-YFP

Protein	Sequence count	Spectral count	Sequence coverage
Atg20	27	59	51.1%
Atg24	17	42	41.6%
Atg24b	15	30	42.8%

Bait: Atg24-YFP

Protein	Sequence count	Spectral count	Sequence coverage
Atg24	42	100	68.8%
Atg20	1	2	3.20%
Mug186	33	87	61.6%

Bait: Atg24b-YFP

Protein	Sequence count	Spectral count	Sequence coverage
Atg24b	38	109	77.7%
Atg20	22	49	49.8%

Bait: Mug186-YFP

Protein	Sequence count	Spectral count	Sequence coverage
Mug186	33	79	64.3%
Atg24	36	92	60.8%

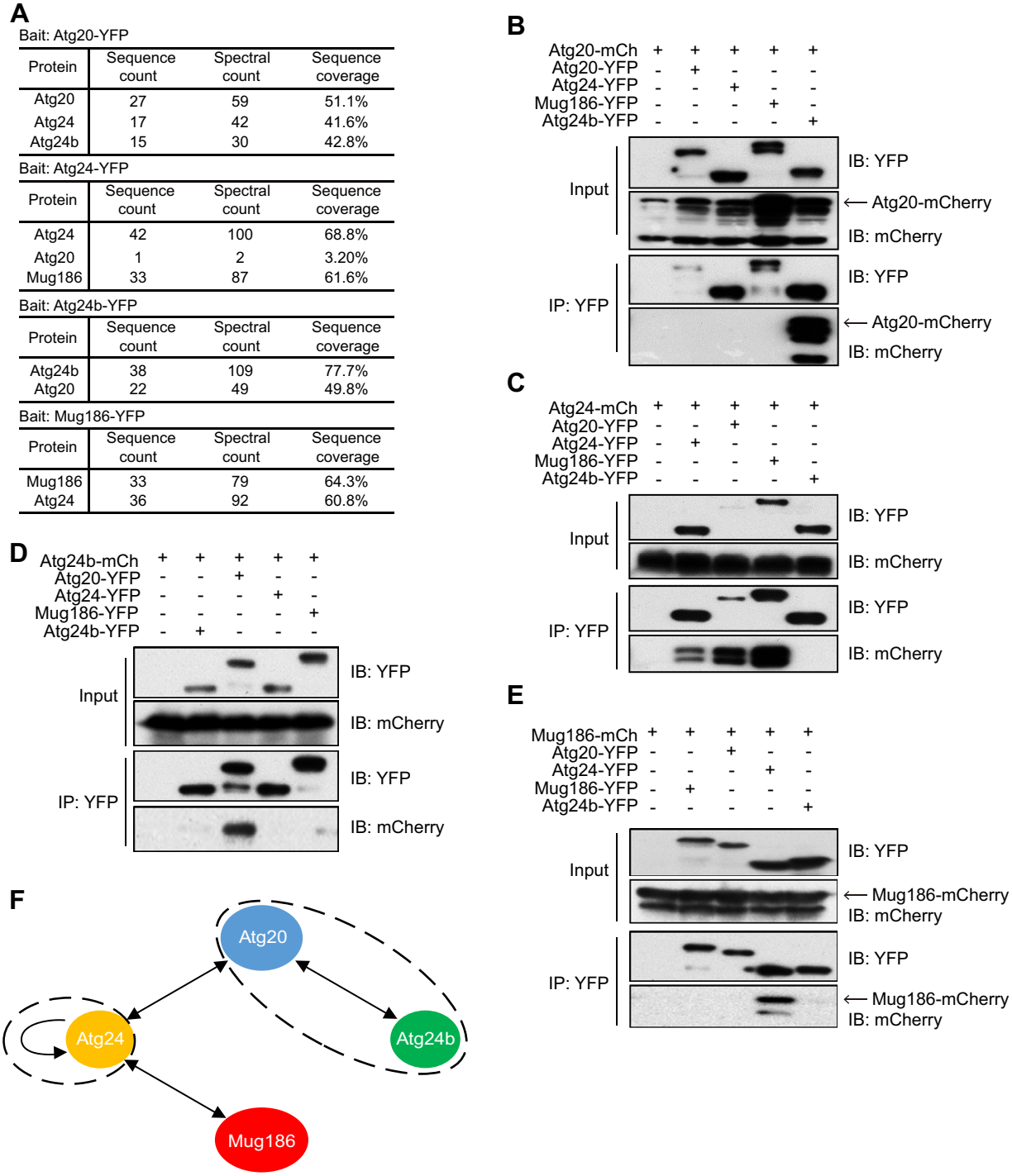

Fig. 5. Atg20- and Atg24-family proteins form multiple oligomers. (A) AP-MS analysis revealed interactions between Atg20- and Atg24-family proteins. Endogenously YFP-tagged Atg20, Atg24, Atg24b and Mug186 were purified using GFP-Trap agarose beads, and bead-bound proteins were identified using mass spectrometry. (B–E) Coimmunoprecipitation analysis to detect possible interactions between YFP-tagged Atg20- and Atg24-family proteins and Atg20–mCherry (B), Atg24–mCherry (C), Atg24b–mCherry (D) and Mug186–mCherry (E). YFP-tagged proteins expressed from the endogenous promoter were immunoprecipitated using GFP-Trap agarose beads, and the coimmunoprecipitation of mCherry-tagged proteins expressed from the *P41nmt1* promoter was analyzed by immunoblotting (IB). IP, immunoprecipitation; mCh, mCherry. (F) A summary of the interactions found between Atg20- and Atg24-family proteins. Arrows represent protein–protein interactions. Dashed ovals indicate the two interactions (Atg20–Atg24b hetero-interaction and Atg24 homo-interaction) that are most likely contribute to the organelle autophagic function.

experiments (Fig. 5B–E). For the Atg20–Atg24b interaction, strong coimmunoprecipitation was observed no matter which protein was used as bait (Fig. 5B,D). The Atg24–Mug186 interaction was also supported by reciprocal coimmunoprecipitation (Fig. 5C,E). For the Atg20–Atg24 pair, strong interaction was only detected when Atg20 was used as bait (Fig. 5B,C), perhaps owing to the C-terminal YFP tag on Atg24 interfering with this interaction. Even though both Atg20 and Mug186 interacted with Atg24, no interaction was found

Journal of Cell Science (2016) 129, 4289-4304 doi:10.1242/jcs.194373

between Atg20 and Mug186, suggesting that Atg24 can engage only one interaction partner at a time. Similarly, no interaction was found between Atg24 and Atg24b, despite both of them being able to interact with Atg20. In addition to the hetero-interactions, the coimmunoprecipitation analysis also revealed that Atg24 can engage in a homotypic interaction (Fig. 5C). Given the results of the mutant-phenotype analysis, we speculate that the functional forms of these proteins are the oligomers (including dimers), and either the homo-oligomer of Atg24 or the hetero-oligomer of Atg20 and Atg24b is sufficient to promote organelle autophagy (Fig. 5F).

No other Atg proteins were found in our AP-MS analysis. Because budding yeast Atg20 and Atg24 interact with Atg17 (Nice et al., 2002), we used a yeast two-hybrid (Y2H) assay to examine whether fission yeast Atg20, Atg24 and Atg24b interact with Atg17 or with several other Atg proteins that could act together with Atg17, including Atg1, Atg11, Atg13 and Atg101. The results were all negative (Fig. S3C).

Fission yeast Atg20- and Atg24-family proteins influence the subcellular localizations of their interaction partners

To further understand the functional relevance of the hetero-interactions between Atg20-family and Atg24-family proteins, we examined whether their subcellular localizations were affected by each other. The only interactions we have observed for Atg24b and Mug186 are their hetero-interactions with Atg20 and Atg24, respectively. Supporting the importance of these interactions, puncta formation by Atg24b was completely abolished in *atg20Δ* cells (Fig. S4A), and puncta formation by Mug186 was completely abolished in *atg24Δ* cells (Fig. S4B). Atg20 can interact with either Atg24 or Atg24b. Under nutrient-rich conditions, Atg20 no longer formed puncta in *atg24Δ* cells (Fig. S4C), consistent with the fact that Atg24 but not Atg24b forms puncta under such conditions. The PAS localization of Atg20 in starved cells remained largely normal in *atg24Δ* or *atg24bΔ* single mutants (Fig. S4C). In contrast, in the *atg24Δ atg24bΔ* double mutant, Atg8-colocalizing Atg20 puncta were severely diminished (Fig. S4C). Thus, the PAS localization of Atg20 redundantly depends on its two interaction partners Atg24 and Atg24b. Atg24 can engage not only in hetero-interactions with Atg20 and Mug186, but also in a homo-interaction with itself. Deleting *mug186* strongly reduced the numbers of puncta formed by Atg24 but did not affect the PAS localization of Atg24, and this deletion actually made it easier to observe the PAS localization of Atg24 than it was to observe in the wild-type cells (Fig. S4D). Deleting *atg20* either in wild-type or *mug186Δ* background did not obviously alter the localization pattern of Atg24 (Fig. S4D), consistent with the model that Atg24 homo-oligomers can function in the absence of both Atg20 and Mug186. The results of these analyses are summarized in Fig. S4E.

Taken together, these localization data suggest that the three hetero-interactions found by using our biochemical analysis, namely, the Atg24–Atg20 interaction, the Atg24–Mug186 interaction and the Atg20–Atg24b interaction, all contribute to the normal localization patterns of the Atg20- and Atg24-family proteins, including their localization at PAS. The autophagy phenotype data shown in Figs 3 and 4 suggest that the Atg20–Atg24b hetero-oligomer functions during organelle autophagy. It remains possible that the Atg24–Atg20 hetero-oligomer and/or the Atg24–Mug186 hetero-oligomer also function in autophagy. However, because Atg24 by itself can support organelle autophagy, testing these possibilities will have to await the creation of separation-of-function *atg24* mutations that abolish the homotypic but not heterotypic interactions.

The loss of Atg24 alone causes a defect in the endosomal sorting of the SNARE protein Syb1

Budding yeast Atg20 and Atg24 have been implicated in not only autophagy, but also in the sorting of a SNARE protein, Snc1, at the endosome (Hettema et al., 2003). It is not entirely clear whether the autophagic function of these proteins is independent of their endosomal sorting function. We examined the localization of the fission yeast Snc1 homolog, Syb1 (Fig. 6). In wild-type cells, GFP–Syb1 concentrated at the cell cortex, in particular at cell tips and septa, as previously reported (Edamatsu and Toyoshima, 2003; Kita et al., 2004). These sites are presumably plasma membrane regions where polarized exocytosis occurs. In addition, we also observed cytoplasmic puncta of Syb1, some of which could represent endosomes through which Syb1 traffics during its recycling (Gachet and Hyams, 2005; He et al., 2006; Kita et al., 2004). Wild-type-like Syb1 localization patterns were observed in single-mutant cells that lacked Atg20, Atg24b or Mug186. In contrast, in *atg24Δ* single-mutant cells, GFP–Syb1 still localized to cytoplasmic puncta but was seldom found concentrated at the cell cortex (Fig. 6), suggesting that Atg24 is important for the proper plasma membrane localization of Syb1, probably due to an endosomal sorting function of Atg24, similar to that of its budding yeast homolog (Hettema et al., 2003). The fact that *atg24Δ* cells showed no defect in ER autophagy (Fig. 3) indicates that impeding endosomal sorting does not cause defects in organelle autophagy. Furthermore, the two double mutants that were defective in organelle autophagy, *atg20Δ atg24Δ* and *atg24Δ atg24bΔ*, did not exhibit more severe Syb1 localization defects than the *atg24Δ* single mutant (Fig. 6). Thus, the autophagy defects of these double mutants do not appear to result from their endosomal sorting defect. However, we cannot rule out the possibility that under starvation conditions, endosomal trafficking is altered so that the double mutants suffer a more severe endosomal transport defect than the *atg24Δ* single mutant. It has been proposed that endosomal trafficking is re-routed in response to starvation in budding yeast (Shirahama-Noda et al., 2013).

A defect in organelle autophagy caused by the loss of Atg20- and Atg24-family proteins is associated with reduced autophagosome size

For organelle autophagy to occur efficiently, autophagosomes need to accommodate the large sizes of the cargos. We hypothesized that Atg20- and Atg24-family proteins might promote organelle autophagy by ensuring autophagosomes are sufficiently large. To investigate this possibility, we examined the size of autophagosomes in mutants that lacked Atg20- and Atg24-family proteins. We used the deletion of the *fsc1* gene to block autophagosome–vacuole fusion so that autophagosomes would accumulate during starvation (Sun et al., 2013). To visualize the accumulated autophagosomes, we employed a fluorescence loss in photobleaching (FLIP) assay (Fig. 7A,B) (Sun et al., 2013). In this assay, repetitive photobleaching at a site near one cell tip diminishes the fluorescence signal of diffusible cytoplasmic Tdh1–YFP but leaves the fluorescence signal of autophagosome-enclosed Tdh1–YFP intact. Introducing into the *fsc1Δ* background the deletion of both *atg24* and *atg24b*, or the deletion of both *atg20* and *atg24*, which hinders organelle autophagy, caused a marked reduction of the autophagosome size; in contrast, the deletion of *atg24* or the double deletion of both *atg20* and *atg24b*, which do not cause an organelle autophagy defect, did not alter or only moderately reduced the size of autophagosomes. Thus, there appears to be a correlation between the severity of the organelle autophagy defect and the extent of autophagosome size reduction. Because fluorescence microscopy has limited spatial resolution, in order to accurately measure

Journal of Cell Science (2016) 129, 4289-4304 doi:10.1242/jcs.194373

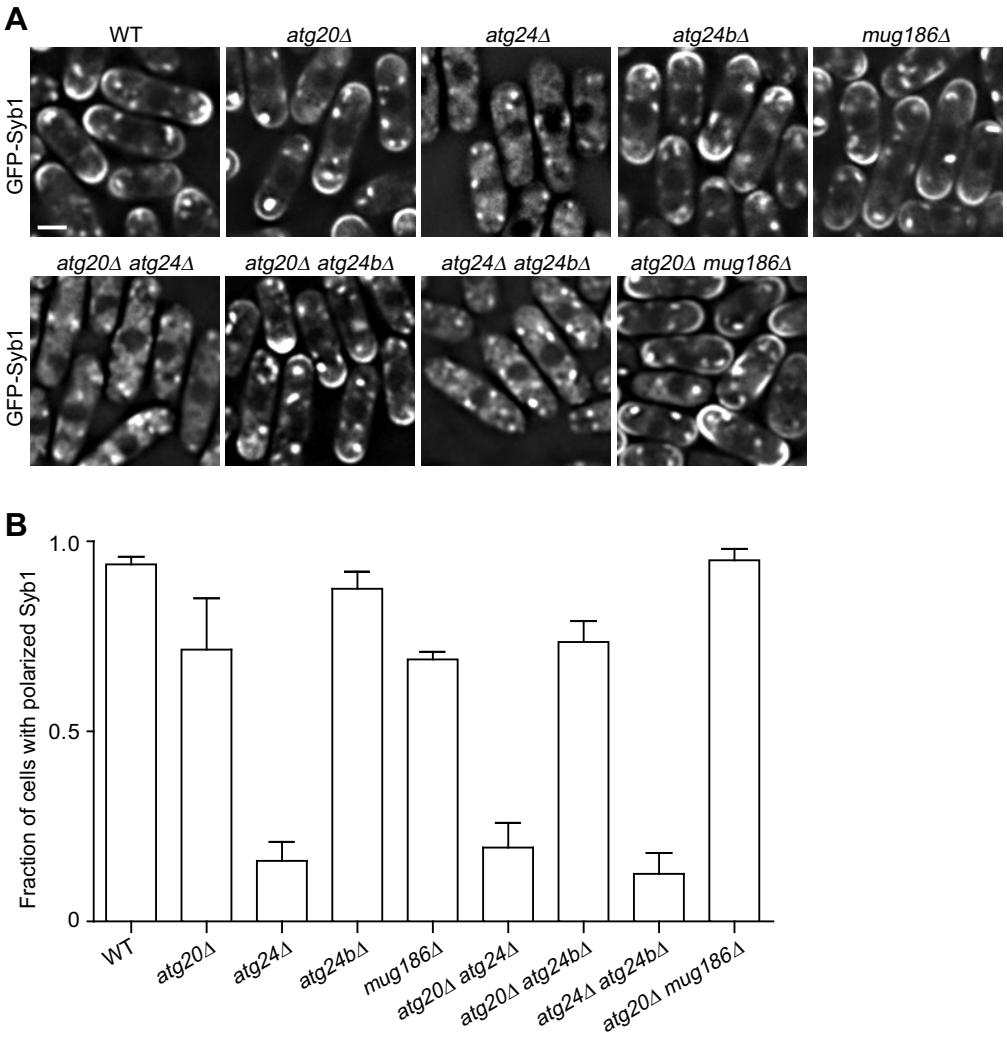

Fig. 6. The *atg24Δ* single mutant is defective in the endosomal sorting of Syb1. (A) Polarized Syb1 localization was diminished in *atg24Δ*, *atg20Δ atg24Δ* and *atg24Δ atg24bΔ*. Cells expressing GFP-tagged Syb1 from the *P41nmt1* promoter were grown to mid-log phase and examined by using fluorescence microscopy. Scale bar: 3 µm. (B) Quantification of the fractions of cells with Syb1–GFP signal at the cell tip or septum (mean±s.e.m.; 100 cells were examined each time). WT, wild type.

autophagosome size, we performed transmission electron microscopy analysis (TEM) (Fig. 7C,D). A significant size difference was observed between the autophagosomes that accumulated in *fsc1Δ* cells and those that accumulated in *fsc1Δ atg20Δ atg24Δ atg24bΔ* cells. The average diameter of autophagosomes in *fsc1Δ* cells was 462 nm, whereas the average diameter of autophagosomes in *fsc1Δ atg20Δ atg24Δ atg24bΔ* cells was 300 nm. Taken together, these data suggest that the organelle autophagy defect caused by the loss of Atg20- and Atg24-family proteins is due to a failure to form autophagosomes of sufficient size.

The organelle autophagy defect caused by the loss of Atg20- and Atg24-family proteins is associated with reduced Atg8 accumulation at the PAS and enhanced Atg9 accumulation at the PAS

When observing CFP–Atg8 puncta, we noticed that the intensities of CFP–Atg8 puncta appeared to differ somewhat between wild type and certain mutants lacking Atg20- and Atg24-family proteins. In budding yeast, Atg8 promotes phagophore expansion and controls the sizes of autophagosomes (Jin and Klionsky, 2014; Nakatogawa et al., 2007; Xie et al., 2008). Thus, we hypothesized that the reduced autophagosome size could be due to a reduced level of Atg8 at the PAS. We quantified the intensities of CFP–Atg8 puncta in starved cells, and found that, indeed, the CFP–Atg8 puncta in mutants that formed smaller autophagosomes were not as bright as the puncta in wild type or mutants that formed relatively normal-sized autophagosomes (Fig. 8A).

Even though the mutants defective in organelle autophagy formed smaller autophagosomes, our Tdh1–YFP-processing data showed that general autophagy remained normal in these mutants. We hypothesized that autophagosome size reduction could be compensated by increased autophagosome number. Thus, we quantified the number of autophagosomes by using the FLIP analysis data and found that, indeed, mutants that formed smaller autophagosomes accumulated more autophagosomes than the wild type (Fig. 8B).

In budding yeast, autophagosome number is controlled by Atg9 (Jin and Klionsky, 2014; Jin et al., 2014). Thus, we examined Atg9 localization (Fig. 8C,D). After starvation, approximately 30% of CFP–Atg8 puncta overlapped with Atg9–YFP puncta in wild-type cells. Significantly higher levels of overlap between CFP–Atg8 puncta and Atg9–YFP puncta were observed for mutants that formed smaller but more numerous autophagosomes, indicating that enhanced Atg9 accumulation at the PAS could underlie the compensatory increase of autophagosome number in mutants defective in organelle autophagy but not in general autophagy.

DISCUSSION

In this study, we established that ER autophagy and mitochondrial autophagy occur in the fission yeast *S. pombe* during nitrogen starvation. We found that Atg20- and Atg24-family proteins are

Journal of Cell Science (2016) 129, 4289-4304 doi:10.1242/jcs.194373

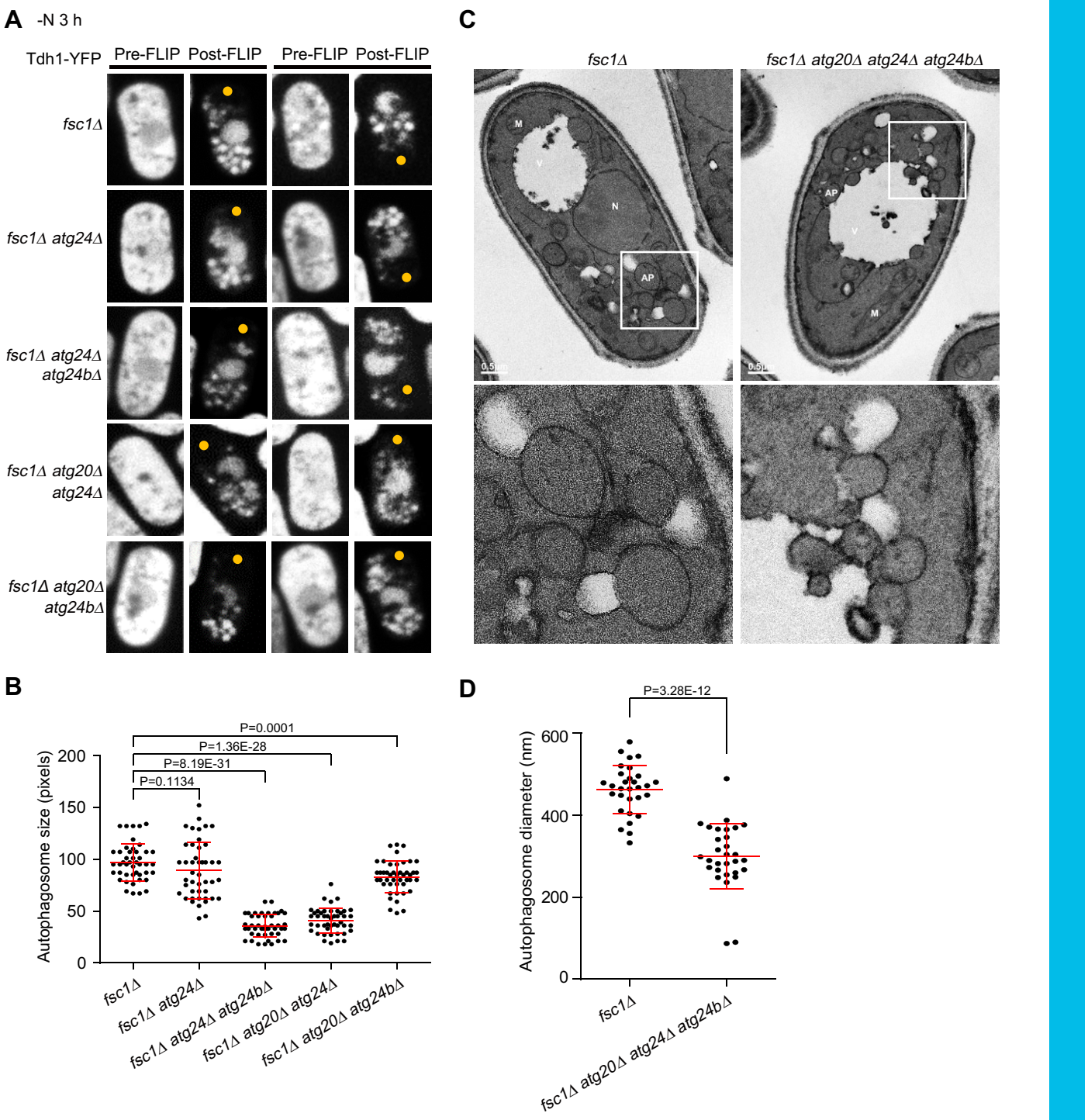

Fig. 7. Mutants defective in organelle autophagy have smaller autophagosomes. (A) Autophagosomes were accumulated using a *fsc1Δ* mutation that blocks autophagosome–vacuole fusion and were rendered visible by fluorescence loss in photobleaching (FLIP) that abolished the diffusible cytoplasmic fluorescent signal of Tdh1–YFP. Besides Tdh1–YFP that was trapped inside autophagosomes, a nuclear pool of Tdh1–YFP also remained visible post FLIP, as shown previously (Sun et al., 2013). Cells expressing YFP-tagged Tdh1 were collected after 3 h of starvation, and the FLIP assay was performed. Yellow dots mark the sites of photobleaching. Two representative cells are shown for each strain. (B) Quantification of the size of autophagosomes observed during the FLIP analysis. The mean±s.d. is shown in red (n=45). *P*-values were calculated using Welch's *t*-test. (C) Representative electron microscopy images of *fsc1Δ* and *fsc1Δ atg20Δ atg24Δ atg24bΔ* cells. N, nucleus; M, mitochondrion; V, vacuole; AP, autophagosome. White squares enclose regions shown at higher magnification below. (D) Quantification of the size of autophagosomes observed in the electron microscopy analysis. The mean±s.d. is shown in red (n=30). *P* values were calculated using Welch's *t*-test.

important for organelle autophagy but are dispensable for general autophagy. Interestingly, these proteins act in a redundant fashion, and thus only two combinations of double mutants but none of the single mutants exhibit defects in organelle autophagy. One of these proteins, Atg24, also functions in endosomal sorting, but this role appears to be separate from its role in autophagy. Our biochemical

Journal of Cell Science (2016) 129, 4289-4304 doi:10.1242/jcs.194373

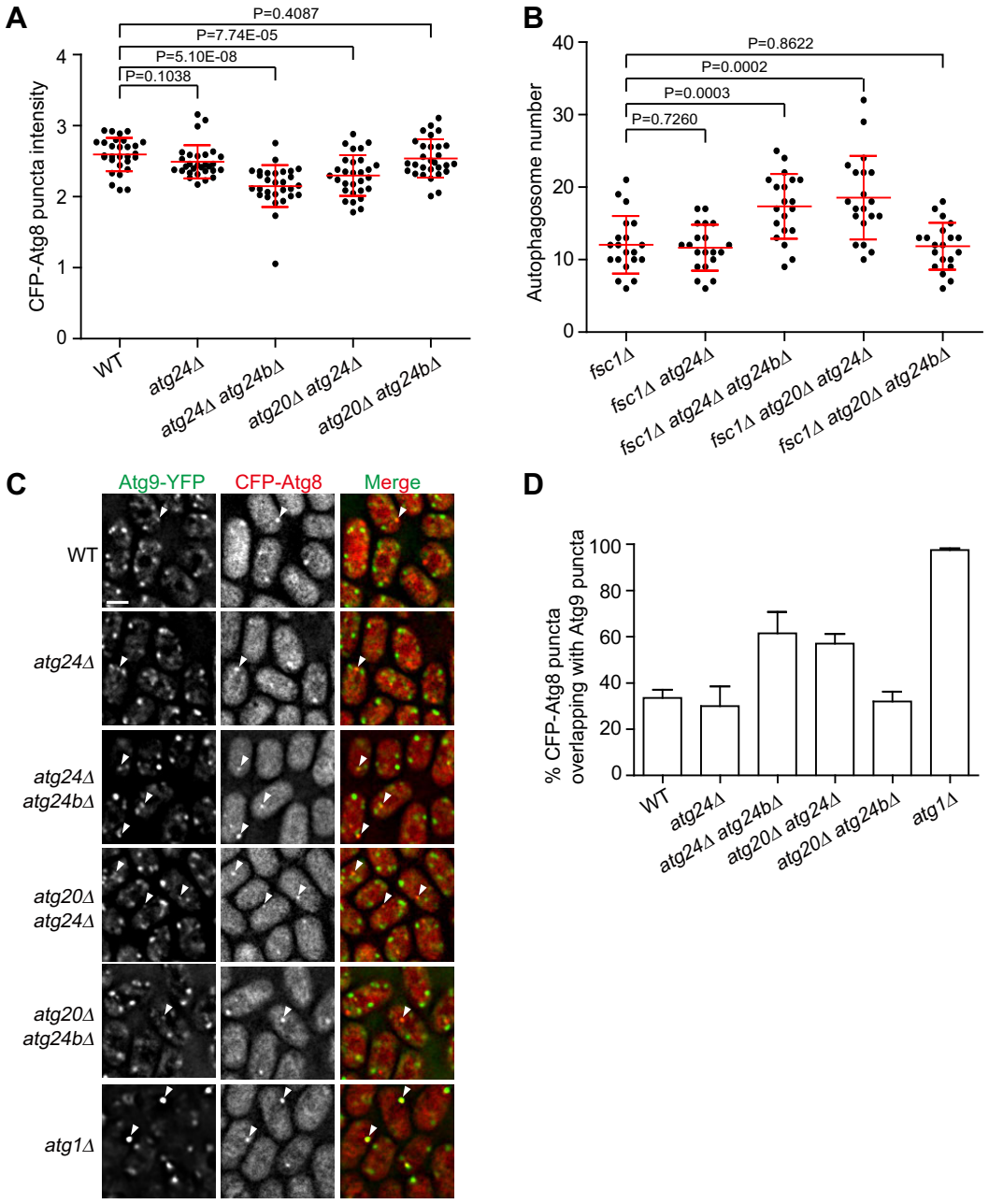

Fig. 8. Mutants defective in organelle autophagy have reduced Atg8 accumulation and enhanced Atg9 accumulation at the PAS. (A) Quantification of the intensity of starvation-induced CFP–Atg8 puncta. Cells expressing endogenously CFP-tagged Atg8 were examined after 2 h of starvation. The values are log10-transformed average pixel intensities in 7×7-pixel regions surrounding the puncta after background subtraction. Mean±s.d. are shown in red (n=30). P-values were calculated using Welch's t-test. (B) Quantification of the numbers of autophagosomes per cell. Images of the FLIP assay shown in Fig. 7A were analyzed. The mean±s.d. are shown in red (n=20). P-values were calculated using Welch's t-test. (C) Localization patterns of Atg9–YFP. Cells expressing endogenously YFP-tagged Atg9 were examined after 2 h of starvation. Arrowheads indicate representative puncta where Atg8 and Atg9 colocalized. Scale bar: 3 µm. (D) Quantification of the percentages of CFP–Atg8 puncta that overlapped with Atg9–YFP puncta in the analysis shown in C (mean±s.e.m.; 100 Atg8 puncta were examined each time). WT, wild type.

analysis revealed one homotypic and three heterotypic interactions among the four Atg20- and Atg24-family proteins, and imaging analysis showed that the heterotypic interactions influence the subcellular localization of these proteins, including their localization at the PAS. Finally, we showed that the underlying cause of the organelle autophagy defect could be a failure to maintain proper autophagosome size.

In budding yeast, ER and mitochondria are cargos of selective autophagy pathways (Kanki and Klionsky, 2008; Kanki et al., 2009a; Mochida et al., 2015; Okamoto et al., 2009). A defining feature of selective autophagy pathways is the requirement for cargo-specificity-determining factors called autophagy receptors (Jin et al., 2013; Khaminets et al., 2016; Rogov et al., 2014). Autophagy receptors link selective cargos to the core autophagy machinery, especially to the Atg8 protein. At least eight autophagy receptors have been identified in fungal species: *S. cerevisiae* Atg19 and Atg34 for the Cvt pathway (Leber et al., 2001; Scott et al., 2001; Suzuki et al., 2010), *S. cerevisiae* Atg30 and *P. pastoris* Atg36 for

Journal of Cell Science (2016) 129, 4289-4304 doi:10.1242/jcs.194373

pexophagy (Farré et al., 2008; Motley et al., 2012), *S. cerevisiae* Atg32 for mitophagy (Kanki et al., 2009a; Okamoto et al., 2009), *S. cerevisiae* Atg39 for nucleophagy (Mochida et al., 2015), *S. cerevisiae* Atg40 for ER-phagy (Mochida et al., 2015) and *S. cerevisiae* Cue5 for aggrephagy (Lu et al., 2014). Among these receptors, only Cue5 has an obvious *S. pombe* homolog (SPBC16E9.02c), which is a yet uncharacterized protein. *S. pombe* Nbr1 is a homolog of mammalian autophagy receptor NBR1 and is distantly related to *S. cerevisiae* Atg19 (Kraft et al., 2010; Liu et al., 2015). However, Nbr1 mediates an unconventional selective autophagy pathway that does not rely on the core autophagy machinery (Liu et al., 2015). Thus, it remains unclear whether conventional autophagy receptors exist in *S. pombe*.

Besides the molecular hallmark of receptor proteins, another criterion that has been applied to distinguish selective and nonselective autophagy pathways is the autophagy-triggering stimuli (Sica et al., 2015). It is commonly believed that starvation-triggered autophagy tends to be nonselective and can randomly engulf any cellular components to meet the heightened demand of cellular material recycling. However, in *S. cerevisiae*, the autophagy of the hydrolase Ams1 and the autophagy of ER under the starvation conditions are receptor-dependent processes (Suzuki et al., 2010; Mochida et al., 2015). Thus, certain cargos appear to be preferentially targeted by selective autophagy even during starvation. It is possible that the starvation-induced organelle autophagy processes we observed in fission yeast are also selective. However, the identification of pathway-specific receptors will be needed to draw definitive conclusions.

We found that Atg24 can self-interact, like its budding yeast ortholog (Nice et al., 2002). In addition, we uncovered three pair-wise hetero-interactions – Atg20–Atg24, Atg20–Atg24b and Atg24–Mug186 interactions. Interestingly, these hetero-interactions all occur between an Atg20-family protein and an Atg24-family protein. This is reminiscent of the situation in the budding yeast, where the Atg20–Atg24 interaction and the Snx41–Atg24 interaction, but not the Snx41–Atg20 interaction, have been detected (Hettema et al., 2003; Nice et al., 2002). Budding yeast Atg20 and Atg24 also engage in other protein–protein interactions, such as their interactions with Atg17 (Nice et al., 2002) and conserved oligomeric Golgi (COG) complex subunits (Yen et al., 2010), and the interaction between Atg20 and Atg11 (Yorimitsu and Klionsky, 2005). However, our AP-MS analysis and pair-wise Y2H analysis failed to detect similar interactions in fission yeast, suggesting that these interactions are either not conserved or difficult to observe under our experimental conditions.

In their well-established roles in the Cvt pathway, pexophagy and mitophagy, budding yeast Atg20 and Atg24 are equally important, presumably because they are only functional when forming a hetero complex together. Fission yeast Atg20 and Atg24b behave similarly, interacting with each other and being equally indispensable for organelle autophagy when Atg24 is absent. Thus, an Atg20-family protein and an Atg24-family protein acting together in a heterotypic complex appears to be a conserved mode of action for these two families of PX-BAR proteins. However, this is not the only way these proteins function. Fission yeast Atg24 is capable of acting alone in the absence of any Atg20-family protein. Budding yeast Atg24 might also adopt such a mode of action under certain situations given that Atg24 but not Atg20 is important for the piecemeal microautophagy of the nucleus (PMN) (Krick et al., 2008), and for the starvation-induced autophagy of fatty acid synthase (Shpilka et al., 2015).

In budding yeast, efficient organelle autophagy requires the participation of organelle fission machinery, suggesting that it is important to match the size of the organelle cargo with the size of the autophagosome (Mao et al., 2013, 2014). We found in this study that an organelle autophagy defect and a reduction of autophagosome size are two correlated phenotypes of mutants that lack Atg20- and Atg24-family proteins. Thus, we propose that a failure to maintain proper autophagosome size is the underlying cause of the organelle autophagy defect. PX-BAR proteins have intrinsic capabilities to sense and induce curvature, and to remodel membranes (van Weering and Cullen, 2014). We speculate that Atg20- and Atg24-family proteins contribute to the regulation of autophagosome size by modulating the membrane curvature of certain regions of the expanding phagophore. Alternatively, through their association with the autophagic membrane, they might alter the local concentrations of certain Atg proteins, such as of Atg8. Further studies using *in vitro* reconstitution systems might provide detailed insights into how these proteins influence autophagosome formation (Brier et al., 2016; Rao et al., 2016).

It has been shown that budding yeast Atg20 and Atg24 contribute to general autophagy, but their roles can be masked by compensatory mechanisms (Ohashi and Munro, 2010). Our observation here that the reduction of autophagosome size caused by the loss of Atg20- and Atg24-family proteins is compensated by an increase of autophagosome numbers suggests that fission yeast Atg20- and Atg24-family proteins also contribute to general autophagy in a way that can be masked by compensatory mechanisms, at least for the soluble cargos.

Previously, it has been shown that Atg20- and Atg24-family proteins in *S. cerevisiae* and *P. pastoris*, two Ascomycota species belonging to the Saccharomycotina subphylum, and those in *Magnaporthe oryzae*, an Ascomycota species belonging to the Pezizomycotina subphylum, are important for organelle autophagy (Nice et al., 2002; Kanki and Klionsky, 2008; Ano et al., 2005; He et al., 2013; Deng et al., 2012). *S. pombe* belongs to Taphrinomycotina, a more basal subphylum of Ascomycota (Stajich et al., 2009). Thus, our findings here provide further evidence that the involvement of Atg20- and Atg24-family proteins in organelle autophagy is evolutionarily conserved. It will be worthwhile to investigate whether their mammalian homologs SNX4, SNX7 and SNX30 also play similar roles in autophagy (van Weering et al., 2010, 2012).

MATERIALS AND METHODS

Fission yeast strains and media

Fission yeast strains used in this study are listed in Table S1. Genetic methods for strain construction and composition of media are as described (Forsburg and Rhind, 2006). An integrating plasmid expressing Ost4–CFP from the *Pnmt1* promoter was constructed by performing a Gateway LR reaction between the ORFeome library entry clone of the *ost4* gene and the pDUAL-CFH1c destination plasmid (Matsuyama et al., 2006). The resulting plasmid was linearized with NotI digestion and integrated at the *leu1* locus. The strain expressing Sdh2–mCherry under the native promoter was constructed by PCR-based tagging. An integrating plasmid expressing mito-mCherry was constructed by inserting sequences encoding the mitochondrial targeting sequence of *S. cerevisiae* Cox4 and mCherry into the integrating vector pHIS3K-Ptub1 (Matsuyama et al., 2008). The resulting plasmid was linearized through NotI digestion and integrated at the *his3* locus. Strains expressing ER-GFP (called GFP-AHDL in previous publications) were provided by Snezhana Oliferenko (King's College London, London, UK) (Zhang et al., 2010). Strains expressing PX-BAR proteins fused with the YFP–FLAG–His6 (YFH) tag from their native promoters were constructed by using an overlap-extension PCR approach (Yu et al., 2013). Strains expressing CFP–Atg8 and Tdh1–YFH were as reported previously (Sun et al., 2013). For the construction of the strain expressing GFP–Syb1, the coding sequence of Syb1 was amplified by

performing PCR from genomic DNA and inserted into a modified pDUAL vector, which contains the *P41nmt1* promoter and the sequence encoding GFP (Wei et al., 2014), and the resulting plasmid was linearized through NotI digestion and integrated at the *leu1* locus. Deletion strains were constructed by performing PCR to amplify the deletion cassettes in the Bioneer deletion strains and transforming the PCR product into strains in our laboratory strain collection.

Processing assay of fluorescent-protein-fused proteins

Cell lysates were prepared from about 5 OD_{600} units of yeast cells using a trichloroacetic acid (TCA) lysis method (Ulrich and Davies, 2009). Samples were separated on 10% SDS-PAGE gels and then immunoblotted with an antibody that can recognize GFP (also YFP and CFP; cat no: 11814460001, Roche; 1:3000) or mCherry tag (cat no: M40012, Abmart; 1:2000). Protein bands were quantified using the 'Analyze tool' in the Fiji distribution of ImageJ software (Schindelin et al., 2012).

Fluorescence microscopy

Except for analysis of the FLIP assay, live-cell imaging was performed using a DeltaVision PersonalDV system (Applied Precision) equipped with an mCherry–GFP–CFP filter set (Chroma 89006 set) and a Photometrics CoolSNAP HQ2 camera. Images were acquired with a 100×, 1.4-NA objective and analyzed with the SoftWoRx software. Punctum intensity was determined by measuring the fluorescence intensities of two concentric square regions (7×7 and 9×9 pixels, respectively) centered around the punctum and by calculating background subtraction using the method described previously in Hoffman et al. (2001).

Immunoprecipitation

Approximately 100 OD_{600} units of log-phase cells was harvested and washed once with water. Cells were lysed by beating with 0.5-mm-diameter glass beads in the lysis buffer (50 mM HEPES, pH 7.5, 150 mM NaCl, 1 mM EDTA, 1 mM DTT, 1 mM PMSF, 0.05% NP-40, 10% glycerol, 1× Roche protease inhibitor cocktail) using a FastPrep-24 instrument. The cell lysate was cleared by centrifugation at 15871 ***g*** for 30 min. The supernatant was incubated with GFP-Trap agarose beads (Chromotek). After incubation, the agarose beads were washed three times with lysis buffer. Proteins that had bound to beads were eluted by boiling in SDS-PAGE loading buffer.

AP-MS analysis

About 1000 OD_{600} units of cells was harvested, and lysate was prepared using the bead-beating lysis method noted above. The supernatant was incubated with GFP-Trap agarose beads for 3 h. After incubation, the agarose beads were washed twice with lysis buffer and another time with lysis buffer that lacked NP-40. Bead-bound proteins were eluted by incubation at 65° with elution buffer (1% SDS, 100 mM Tris-HCl, pH 8.0). Eluted proteins were precipitated with 20% TCA for 1 h. Protein precipitates were washed three times using ice-cold acetone and dissolved in 8 M urea, 100 mM Tris-HCl, pH 8.5, then reduced with 5 mM tris(2-carboxyethyl) phosphine (TCEP) for 20 min, and alkylated with 10 mM iodoacetamide for 15 min in the dark. Then, the samples were diluted by a factor of four and digested overnight at 37° with trypsin (dissolved in 2 M urea, 1 mM $CaCl_2$, 100 mM Tris-HCl, pH 8.5). Formic acid was added to the final concentration of 5% to stop the digestion reaction. After digestion, the LC-MS/MS analysis was performed on an Easy-nLC II HPLC instrument (Thermo Fisher Scientific) coupled to an LTQ Orbitrap XL mass spectrometer (Thermo Fisher Scientific). Peptides were loaded on a pre-column (100 µM ID, 4 cm long, packed with C12 10-µm 120-Å resin from YMC) and separated on an analytical column (75 µM inner diameter, 10 cm long, packed with Luna C18 3-µm 100-Å resin from Phenomenex) using an acetonitrile gradient 0–28% in 100 min at a flow rate of 200 nl/min. The top eight most intense precursor ions from each full scan (resolution 60,000) were isolated for collision induced dissociation tandem mass spectrometry spectra analysis (CID MS2) (normalized collision energy 35) with a dynamic exclusion time of 60 s. Tandem mass spectrometry fragment ions were detected by using linear ion trap in a normal scan mode. Precursors with charge states that were unassigned or less than 2+ were excluded. The tandem mass spectrometry spectra were searched with Prolucid software against an *S. pombe* protein database. The search results were filtered with DTASelect software.

FLIP assay

The photobleaching of the Tdh1–YFP signal and image acquisition were performed with a PerkinElmer Ultraview VoX spinning-disc system, using a 100× objective. Quantitative analysis of autophagosome size was performed with the Volocity software.

Electron microscopy

Approximately 100 OD_{600} units of cells were starved for 3 h and harvested, then washed once with 10 ml of water. The samples were fixed with 2% glutaraldehyde and 4% $KMnO_4$, then dehydrated through a graded ethanol series and embedded in Spurr's resin. Thin sections were examined using an FEI Tecnai G2 Spirit electron microscope equipped with a Gatan 895 4k×4k CCD camera. The sizes of autophagosomes were determined using a method previously used for measuring autophagic body size (Xie et al., 2008).

Acknowledgements

We thank Snezhana Oliferenko for providing the ER-GFP (GFP-AHDL) strains, Meng Ouyang for constructing the mito-mCherry plasmid, Jia-Min Zhang for help constructing the Sdh2–mCherry strains, Wan-Zhong He for help with electron microscopy.

Competing interests

The authors declare no competing or financial interests.

Author contributions

D.Z. performed most of the experiments and prepared the manuscript; X.-M.L., Z.-Q.Y. and L.-L.S. performed some of the experiments; X. X. and M.-Q.D. contributed to the mass spectrometry analysis; L.-L.D. conceived the study and participated in the writing of the manuscript.

Funding

This work was supported by the National Basic Research Program of China (Ministry of Science and Technology of the People's Republic of China; 973 Program, 2014CB849901 and 2014CB849801), and by grants from the Ministry of Science and Technology of the People's Republic of China and the Beijing municipal government to M.-Q.D. and L.-L.D.

Supplementary information

Supplementary information available online at
http://jcs.biologists.org/lookup/doi/10.1242/jcs.194373.supplemental

References

Ano, Y., Hattori, T., Oku, M., Mukaiyama, H., Baba, M., Ohsumi, Y., Kato, N. and Sakai, Y. (2005). A sorting nexin PpAtg24 regulates vacuolar membrane dynamics during pexophagy via binding to phosphatidylinositol-3-phosphate. *Mol. Biol. Cell* **16**, 446-457.

Brier, L. W., Zhang, M. and Ge, L. (2016). Mechanistically dissecting autophagy: insights from in vitro reconstitution. *J. Mol. Biol.* **428**, 1700-1713.

Deng, Y. Z., Qu, Z., He, Y. and Naqvi, N. I. (2012). Sorting nexin Snx41 is essential for conidiation and mediates glutathione-based antioxidant defense during invasive growth in Magnaporthe oryzae. *Autophagy* **8**, 1058-1070.

Deng, Y., Qu, Z. and Naqvi, N. I. (2013). The role of snx41-based pexophagy in magnaporthe development. *PLoS ONE* **8**, e79128.

Edamatsu, M. and Toyoshima, Y. Y. (2003). Fission yeast synaptobrevin is involved in cytokinesis and cell elongation. *Biochem. Biophys. Res. Commun.* **301**, 641-645.

Farré, J.-C., Manjithaya, R., Mathewson, R. D. and Subramani, S. (2008). PpAtg30 tags peroxisomes for turnover by selective autophagy. *Dev. Cell* **14**, 365-376.

Feng, Y., He, D., Yao, Z. and Klionsky, D. J. (2014). The machinery of macroautophagy. *Cell Res.* **24**, 24-41.

Forsburg, S. L. and Rhind, N. (2006). Basic methods for fission yeast. *Yeast* **23**, 173-183.

Gachet, Y. and Hyams, J. S. (2005). Endocytosis in fission yeast is spatially associated with the actin cytoskeleton during polarised cell growth and cytokinesis. *J. Cell Sci.* **118**, 4231-4242.

He, Y., Sugiura, R., Ma, Y., Kita, A., Deng, L., Takegawa, K., Matsuoka, K., Shuntoh, H. and Kuno, T. (2006). Genetic and functional interaction between

Ryh1 and Ypt3: two Rab GTPases that function in S. pombe secretory pathway. *Genes Cells* **11**, 207-221.
He, Y., Deng, Y. Z. and Naqvi, N. I. (2013). Atg24-assisted mitophagy in the foot cells is necessary for proper asexual differentiation in Magnaporthe oryzae. *Autophagy* **9**, 1818-1827.
Hettema, E. H., Lewis, M. J., Black, M. W. and Pelham, H. R. B. (2003). Retromer and the sorting nexins Snx4/41/42 mediate distinct retrieval pathways from yeast endosomes. *EMBO J.* **22**, 548-557.
Hoffman, D. B., Pearson, C. G., Yen, T. J., Howell, B. J. and Salmon, E. D. (2001). Microtubule-dependent changes in assembly of microtubule motor proteins and mitotic spindle checkpoint proteins at PtK1 kinetochores. *Mol. Biol. Cell* **12**, 1995-2009.
Hoffman, C. S., Wood, V. and Fantes, P. A. (2015). An ancient yeast for young geneticists: a primer on the Schizosaccharomyces pombe Model System. *Genetics* **201**, 403-423.
Inoue, Y. and Klionsky, D. J. (2010). Regulation of macroautophagy in Saccharomyces cerevisiae. *Semin. Cell Dev. Biol.* **21**, 664-670.
Jiang, P. and Mizushima, N. (2014). Autophagy and human diseases. *Cell Res.* **24**, 69-79.
Jin, M. and Klionsky, D. J. (2014). Regulation of autophagy: modulation of the size and number of autophagosomes. *FEBS Lett.* **588**, 2457-2463.
Jin, M., Liu, X. and Klionsky, D. J. (2013). SnapShot: selective autophagy. *Cell* **152**, 368-368.e2.
Jin, M., He, D., Backues, S. K., Freeberg, M. A., Liu, X., Kim, J. K. and Klionsky, D. J. (2014). Transcriptional regulation by Pho23 modulates the frequency of autophagosome formation. *Curr. Biol.* **24**, 1314-1322.
Kanki, T. and Klionsky, D. J. (2008). Mitophagy in yeast occurs through a selective mechanism. *J. Biol. Chem.* **283**, 32386-32393.
Kanki, T., Wang, K., Cao, Y., Baba, M. and Klionsky, D. J. (2009a). Atg32 is a mitochondrial protein that confers selectivity during mitophagy. *Dev. Cell* **17**, 98-109.
Kanki, T., Wang, K., Baba, M., Bartholomew, C. R., Lynch-Day, M. A., Du, Z., Geng, J., Mao, K., Yang, Z., Yen, W.-L. et al. (2009b). A genomic screen for yeast mutants defective in selective mitochondria autophagy. *Mol. Biol. Cell* **20**, 4730-4738.
Khaminets, A., Behl, C. and Dikic, I. (2016). Ubiquitin-dependent and independent signals in selective autophagy. *Trends Cell Biol.* **26**, 6-16.
Kihara, A., Noda, T., Ishihara, N. and Ohsumi, Y. (2001). Two distinct Vps34 phosphatidylinositol 3-kinase complexes function in autophagy and carboxypeptidase Y sorting in Saccharomyces cerevisiae. *J. Cell Biol.* **152**, 519-530.
Kita, A., Sugiura, R., Shoji, H., He, Y., Deng, L., Lu, Y., Sio, S. O., Takegawa, K., Sakaue, M., Shuntoh, H. et al. (2004). Loss of Apm1, the micro1 subunit of the clathrin-associated adaptor-protein-1 complex, causes distinct phenotypes and synthetic lethality with calcineurin deletion in fission yeast. *Mol. Biol. Cell* **15**, 2920-2931.
Kohda, T. A., Tanaka, K., Konomi, M., Sato, M., Osumi, M. and Yamamoto, M. (2007). Fission yeast autophagy induced by nitrogen starvation generates a nitrogen source that drives adaptation processes. *Genes Cells* **12**, 155-170.
Kraft, C., Peter, M. and Hofmann, K. (2010). Selective autophagy: ubiquitin-mediated recognition and beyond. *Nat. Cell Biol.* **12**, 836-841.
Krick, R., Muehe, Y., Prick, T., Bremer, S., Schlotterhose, P., Eskelinen, E.-L., Millen, J., Goldfarb, D. S. and Thumm, M. (2008). Piecemeal microautophagy of the nucleus requires the core macroautophagy genes. *Mol. Biol. Cell* **19**, 4492-4505.
Leber, R., Silles, E., Sandoval, I. V. and Mazón, M. J. (2001). Yol082p, a novel CVT protein involved in the selective targeting of aminopeptidase I to the yeast vacuole. *J. Biol. Chem.* **276**, 29210-29217.
Liu, X.-M., Sun, L.-L., Hu, W., Ding, Y.-H., Dong, M.-Q. and Du, L.-L. (2015). ESCRTs Cooperate with a Selective Autophagy Receptor to Mediate Vacuolar Targeting of Soluble Cargos. *Mol. Cell* **59**, 1035-1042.
Lu, K., Psakhye, I. and Jentsch, S. (2014). Autophagic clearance of polyQ proteins mediated by ubiquitin-Atg8 adaptors of the conserved CUET protein family. *Cell* **158**, 549-563.
Mao, K., Wang, K., Liu, X. and Klionsky, D. J. (2013). The scaffold protein Atg11 recruits fission machinery to drive selective mitochondria degradation by autophagy. *Dev. Cell* **26**, 9-18.
Mao, K., Liu, X., Feng, Y. and Klionsky, D. J. (2014). The progression of peroxisomal degradation through autophagy requires peroxisomal division. *Autophagy* **10**, 652-661.
Matsuyama, A., Arai, R., Yashiroda, Y., Shirai, A., Kamata, A., Sekido, S., Kobayashi, Y., Hashimoto, A., Hamamoto, M., Hiraoka, Y. et al. (2006). ORFeome cloning and global analysis of protein localization in the fission yeast Schizosaccharomyces pombe. *Nat. Biotechnol.* **24**, 841-847.
Matsuyama, A., Shirai, A. and Yoshida, M. (2008). A novel series of vectors for chromosomal integration in fission yeast. *Biochem. Biophys. Res. Commun.* **374**, 315-319.
McDowall, M. D., Harris, M. A., Lock, A., Rutherford, K., Staines, D. M., Bähler, J., Kersey, P. J., Oliver, S. G. and Wood, V. (2015). PomBase 2015: updates to the fission yeast database. *Nucleic Acids Res.* **43**, D656-D661.
Mizushima, N., Yoshimori, T. and Ohsumi, Y. (2011). The role of Atg proteins in autophagosome formation. *Annu. Rev. Cell Dev. Biol.* **27**, 107-132.
Mochida, K., Oikawa, Y., Kimura, Y., Kirisako, H., Hirano, H., Ohsumi, Y. and Nakatogawa, H. (2015). Receptor-mediated selective autophagy degrades the endoplasmic reticulum and the nucleus. *Nature* **522**, 359-362.
Morigasaki, S., Shimada, K., Ikner, A., Yanagida, M. and Shiozaki, K. (2008). Glycolytic enzyme GAPDH promotes peroxide stress signaling through multistep phosphorelay to a MAPK cascade. *Mol. Cell* **30**, 108-113.
Motley, A. M., Nuttall, J. M. and Hettema, E. H. (2012). Pex3-anchored Atg36 tags peroxisomes for degradation in Saccharomyces cerevisiae. *EMBO J.* **31**, 2852-2868.
Mukaiyama, H., Kajiwara, S., Hosomi, A., Giga-Hama, Y., Tanaka, N., Nakamura, T. and Takegawa, K. (2009). Autophagy-deficient Schizosaccharomyces pombe mutants undergo partial sporulation during nitrogen starvation. *Microbiology* **155**, 3816-3826.
Nakatogawa, H., Ichimura, Y. and Ohsumi, Y. (2007). Atg8, a ubiquitin-like protein required for autophagosome formation, mediates membrane tethering and hemifusion. *Cell* **130**, 165-178.
Nice, D. C., Sato, T. K., Stromhaug, P. E., Emr, S. D. and Klionsky, D. J. (2002). Cooperative binding of the cytoplasm to vacuole targeting pathway proteins, Cvt13 and Cvt20, to phosphatidylinositol 3-phosphate at the pre-autophagosomal structure is required for selective autophagy. *J. Biol. Chem.* **277**, 30198-30207.
Ohashi, Y. and Munro, S. (2010). Membrane delivery to the yeast autophagosome from the Golgi-endosomal system. *Mol. Biol. Cell* **21**, 3998-4008.
Ohsumi, Y. (2014). Historical landmarks of autophagy research. *Cell Res.* **24**, 9-23.
Okamoto, K. (2014). Organellophagy: eliminating cellular building blocks via selective autophagy. *J. Cell Biol.* **205**, 435-445.
Okamoto, K., Kondo-Okamoto, N. and Ohsumi, Y. (2009). Mitochondria-anchored receptor Atg32 mediates degradation of mitochondria via selective autophagy. *Dev. Cell* **17**, 87-97.
Rao, Y., Matscheko, N. and Wollert, T. (2016). Autophagy in the test tube In vitro reconstitution of aspects of autophagosome biogenesis. *FEBS J.* **283**, 2034-2043.
Rogov, V., Dötsch, V., Johansen, T. and Kirkin, V. (2014). Interactions between autophagy receptors and ubiquitin-like proteins form the molecular basis for selective autophagy. *Mol. Cell* **53**, 167-178.
Schindelin, J., Arganda-Carreras, I., Frise, E., Kaynig, V., Longair, M., Pietzsch, T., Preibisch, S., Rueden, C., Saalfeld, S., Schmid, B. et al. (2012). Fiji: an open-source platform for biological-image analysis. *Nat. Methods* **9**, 676-682.
Scott, S. V., Guan, J., Hutchins, M. U., Kim, J. and Klionsky, D. J. (2001). Cvt19 is a receptor for the cytoplasm-to-vacuole targeting pathway. *Mol. Cell* **7**, 1131-1141.
Shirahama-Noda, K., Kira, S., Yoshimori, T. and Noda, T. (2013). TRAPPIII is responsible for vesicular transport from early endosomes to Golgi, facilitating Atg9 cycling in autophagy. *J. Cell Sci.* **126**, 4963-4973.
Shpilka, T., Welter, E., Borovsky, N., Amar, N., Shimron, F., Peleg, Y. and Elazar, Z. (2015). Fatty acid synthase is preferentially degraded by autophagy upon nitrogen starvation in yeast. *Proc. Natl. Acad. Sci. USA* **112**, 1434-1439.
Sica, V., Galluzzi, L., Bravo-San Pedro, J. M., Izzo, V., Maiuri, M. C. and Kroemer, G. (2015). Organelle-specific initiation of autophagy. *Mol. Cell* **59**, 522-539.
Stajich, J. E., Berbee, M. L., Blackwell, M., Hibbett, D. S., James, T. Y., Spatafora, J. W. and Taylor, J. W. (2009). The fungi. *Curr. Biol.* **19**, R840-R845.
Sun, L.-L., Li, M., Suo, F., Liu, X.-M., Shen, E.-Z., Yang, B., Dong, M.-Q., He, W.-Z. and Du, L.-L. (2013). Global analysis of fission yeast mating genes reveals new autophagy factors. *PLoS Genet.* **9**, e1003715.
Suzuki, K. and Ohsumi, Y. (2010). Current knowledge of the pre-autophagosomal structure (PAS). *FEBS Lett.* **584**, 1280-1286.
Suzuki, K., Kondo, C., Morimoto, M. and Ohsumi, Y. (2010). Selective transport of alpha-mannosidase by autophagic pathways: identification of a novel receptor, Atg34p. *J. Biol. Chem.* **285**, 30019-30025.
Tabuchi, M., Iwaihara, O., Ohtani, Y., Ohuchi, N., Sakurai, J., Morita, T., Iwahara, S. and Takegawa, K. (1997). Vacuolar protein sorting in fission yeast: cloning, biosynthesis, transport, and processing of carboxypeptidase Y from Schizosaccharomyces pombe. *J. Bacteriol.* **179**, 4179-4189.
Takeda, K., Yoshida, T., Kikuchi, S., Nagao, K., Kokubu, A., Pluskal, T., Villar-Briones, A., Nakamura, T. and Yanagida, M. (2010). Synergistic roles of the proteasome and autophagy for mitochondrial maintenance and chronological lifespan in fission yeast. *Proc. Natl. Acad. Sci. USA* **107**, 3540-3545.
Teasdale, R. D. and Collins, B. M. (2012). Insights into the PX (phox-homology) domain and SNX (sorting nexin) protein families: structures, functions and roles in disease. *Biochem. J.* **441**, 39-59.
Ulrich, H. D. and Davies, A. A. (2009). In vivo detection and characterization of sumoylation targets in Saccharomyces cerevisiae. *Methods Mol. Biol.* **497**, 81-103.
van Weering, J. R. T. and Cullen, P. J. (2014). Membrane-associated cargo recycling by tubule-based endosomal sorting. *Semin. Cell Dev. Biol.* **31**, 40-47.
van Weering, J. R. T., Verkade, P. and Cullen, P. J. (2010). SNX-BAR proteins in phosphoinositide-mediated, tubular-based endosomal sorting. *Semin. Cell Dev. Biol.* **21**, 371-380.
van Weering, J. R. T., Sessions, R. B., Traer, C. J., Kloer, D. P., Bhatia, V. K., Stamou, D., Carlsson, S. R., Hurley, J. H. and Cullen, P. J. (2012). Molecular

basis for SNX-BAR-mediated assembly of distinct endosomal sorting tubules. *EMBO J.* **31**, 4466-4480.

Wei, Y., Wang, H.-T., Zhai, Y., Russell, P. and Du, L.-L. (2014). Mdb1, a fission yeast homolog of human MDC1, modulates DNA damage response and mitotic spindle function. *PLoS ONE* **9**, e97028.

Welinder, C. and Ekblad, L. (2011). Coomassie staining as loading control in Western blot analysis. *J. Proteome Res.* **10**, 1416-1419.

Xie, Z. and Klionsky, D. J. (2007). Autophagosome formation: core machinery and adaptations. *Nat. Cell Biol.* **9**, 1102-1109.

Xie, Z., Nair, U. and Klionsky, D. J. (2008). Atg8 controls phagophore expansion during autophagosome formation. *Mol. Biol. Cell* **19**, 3290-3298.

Yaffe, M. P., Stuurman, N. and Vale, R. D. (2003). Mitochondrial positioning in fission yeast is driven by association with dynamic microtubules and mitotic spindle poles. *Proc. Natl. Acad. Sci. USA* **100**, 11424-11428.

Yanagida, M., Ikai, N., Shimanuki, M. and Sajiki, K. (2011). Nutrient limitations alter cell division control and chromosome segregation through growth-related kinases and phosphatases. *Philos. Trans. R. Soc. Lond. B Biol. Sci.* **366**, 3508-3520.

Yen, W.-L., Shintani, T., Nair, U., Cao, Y., Richardson, B. C., Li, Z., Hughson, F. M., Baba, M. and Klionsky, D. J. (2010). The conserved oligomeric Golgi complex is involved in double-membrane vesicle formation during autophagy. *J. Cell Biol.* **188**, 101-114.

Yorimitsu, T. and Klionsky, D. J. (2005). Atg11 links cargo to the vesicle-forming machinery in the cytoplasm to vacuole targeting pathway. *Mol. Biol. Cell* **16**, 1593-1605.

Young, P. G. and Fantes, P. A. (1987). Schizosaccharomyces pombe mutants affected in their division response to starvation. *J. Cell Sci.* **88**, 295-304.

Yu, Y., Ren, J.-Y., Zhang, J.-M., Suo, F., Fang, X.-F., Wu, F. and Du, L.-L. (2013). A proteome-wide visual screen identifies fission yeast proteins localizing to DNA double-strand breaks. *DNA Repair* **12**, 433-443.

Zhang, D., Vjestica, A. and Oliferenko, S. (2010). The cortical ER network limits the permissive zone for actomyosin ring assembly. *Curr. Biol.* **20**, 1029-1034.

Zhang, D., Vjestica, A. and Oliferenko, S. (2012). Plasma membrane tethering of the cortical ER necessitates its finely reticulated architecture. *Curr. Biol.* **22**, 2048-2052.